

Accuracy assessments of aerosol optical properties retrieved from Aerosol Robotic Network (AERONET) Sun and sky radiance measurements

O. Dubovik,^{1,2} A. Smirnov,^{1,2} B. N. Holben,¹ M. D. King,³ Y. J. Kaufman,⁴
T. F. Eck,^{1,5} and I. Slutsker^{1,2}

Abstract. Sensitivity studies are conducted regarding aerosol optical property retrieval from radiances measured by ground-based Sun-sky scanning radiometers of the Aerosol Robotic Network (AERONET). These studies focus on testing a new inversion concept for simultaneously retrieving aerosol size distribution, complex refractive index, and single-scattering albedo from spectral measurements of direct and diffuse radiation. The perturbations of the inversion resulting from random errors, instrumental offsets, and known uncertainties in the atmospheric radiation model are analyzed. Sun or sky channel miscalibration, inaccurate azimuth angle pointing during sky radiance measurements, and inaccuracy in accounting for surface reflectance are considered as error sources. The effects of these errors on the characterization of three typical and optically distinct aerosols with bimodal size distributions (weakly absorbing water-soluble aerosol, absorbing biomass-burning aerosol, and desert dust) are considered. The aerosol particles are assumed in the retrieval to be polydispersed homogeneous spheres with the same complex refractive index. Therefore we also examined how inversions with such an assumption bias the retrievals in the case of nonspherical dust aerosols and in the case of externally or internally mixed spherical particles with different refractive indices. The analysis shows successful retrieval of all aerosol characteristics (size distribution, complex refractive index, and single-scattering albedo), provided the inversion includes the data combination of spectral optical depth together with sky radiances in the full solar almucantar (with angular coverage of scattering angles up to 100° or more). The retrieval accuracy is acceptable for most remote sensing applications even in the presence of rather strong systematic or random uncertainties in the measurements. The major limitations relate to the characterization of low optical depth situations for all aerosol types, where high relative errors may occur in the direct radiation measurements of aerosol optical depth. Also, the results of tests indicate that a decrease of angular coverage of scattering (scattering angles of 75° or less) in the sky radiance results in the loss of practical information about refractive index. Accurate azimuth angle pointing is critical for the characterization of dust. Scattering by nonspherical dust particles requires special analysis, whereby approximation of the aerosol by spheres allows us to derive single-scattering albedo by inverting spectral optical depth together with sky radiances in the full solar almucantar. Inverting sky radiances measured in the first 40° scattering angle only, where nonspherical effects are minor, results in accurate retrievals of aerosol size distributions of nonspherical particles.

1. Introduction

Much of the current uncertainty in the quantitative assessment of the radiative energy balance of the Earth is due to our lack of knowledge of the radiative impact of aerosols. An improved understanding of the role of aerosols is imperative if

both the natural and anthropogenic-induced trends in climate are to be disentangled. Aerosols have a direct effect on the radiative balance of the Earth by scattering and absorbing both solar and terrestrial radiation.

The difficulties in accessing the contribution of aerosols to radiative processes are caused by incomplete knowledge of aerosol macrophysical properties (sources, sinks, and loading) and of aerosol microphysical properties (composition, size distribution, chemical interaction, lifetime, and diurnal variation). The discrete spatial and temporal nature of both natural (e.g., volcanic eruption, wind-lofted (e.g., Saharan) dust, and sea spray) and anthropogenic aerosol injection (e.g., biomass burning and industrial pollution) makes the problem particularly challenging.

The launch of NASA's Earth Observing System (EOS) and other international satellite platforms equipped with a new generation of sensors is expected to reduce the existing aerosol

¹Laboratory for Terrestrial Physics, NASA Goddard Space Flight Center, Greenbelt, Maryland.

²Also at Science Systems and Applications, Inc., Lanham, Maryland.

³Earth Science Directorate, NASA Goddard Space Flight Center, Greenbelt, Maryland.

⁴Laboratory for Atmospheres, NASA Goddard Space Flight Center, Greenbelt, Maryland.

⁵Also at Raytheon ITSS, Lanham, Maryland.

Copyright 2000 by the American Geophysical Union.

Paper number 2000JD900040.
0148-0227/00/2000JD900040\$09.00

uncertainty in radiative forcing estimates [King *et al.*, 1999]. To validate the remote sensing algorithms and ensure the quality of aerosol products, various ground-based remote sensing measurements as well as some airborne measurements will be conducted. For instance, for highly variable troposphere aerosol the ground-based observations must be performed as close as possible to the satellite overpass.

The Aerosol Robotic Network (AERONET [Holben *et al.*, 1998]), an optical ground-based aerosol monitoring network and data archive, has been initiated by NASA's EOS and expanded by federation with many non-NASA institutions. The network hardware consists of identical automatic Sun-sky scanning spectral radiometers owned by national agencies and universities. Data from this network provide globally distributed near-real time observations of aerosol spectral optical depths, aerosol size distributions, etc., in a manner suitable for integration with satellite data.

Validating aerosol products obtained from various satellite sensors may need ground-based measurements of a variety of optical aerosol characteristics with different data quality requirements. Therefore the error analysis and quality assurance of AERONET products is a question of great importance. AERONET has been developed to provide the aerosol information from two kinds of measurements: spectral data of direct Sun radiation extinction (i.e., aerosol optical depth) and angular distribution of sky radiance.

The optical depth is a very valuable aerosol characteristic, which is a key parameter for various aerosol-related studies, such as aerosol radiative forcing, atmospheric corrections of the aerosol effect on remote sensing, etc. [Kaufman *et al.*, 1997]. The quality of optical depth data from the ground mainly depends on the instrumental design, calibration, and correct identification of clear sky conditions. The details of AERONET instrumentation and operational procedures of the data registration are given in the paper of Holben *et al.* [1998]. The methodology and justification of the cloud screening and the quality control of optical depth for the AERONET database are given by Smimov *et al.* [2000a].

The angular distribution of sky radiance measured from the ground is not the characteristic commonly used for validating satellite or other measurements of aerosol radiative effect. However, the angular distribution of sky radiance contains information that is essential for the retrieval of the aerosol phase function [Nakajima *et al.*, 1983, 1996] and single-scattering albedo (defining the degree of absorption) [Holben *et al.*, 1996; Devaux *et al.*, 1998; Dubovik *et al.*, 1998a]. These two parameters are complementary characteristics to optical depth for a comprehensive consideration of aerosol radiative transfer properties. In addition, important aerosol microphysical parameters, such as the particle size distribution [Nakajima *et al.*, 1983, 1996] and complex refractive index, can be derived with the use of sky radiance measurements [Wendish and von Hoyningen-Huene, 1994; Yamasoe *et al.*, 1998; O. Dubovik and M. D. King, A flexible inversion algorithm for retrieval of aerosol optical properties from Sun and sky radiance measurements, submitted to the *Journal of Geophysical Research*, 1999 (hereinafter referred to as Dubovik and King, submitted manuscript, 1999)].

The present inversion algorithm employed by AERONET [Nakajima *et al.*, 1983, 1996] retrieves only the volume size distribution [Holben *et al.*, 1998]. In specific cases other aerosol parameters, such as single-scattering albedo [Holben *et al.*, 1996; Dubovik *et al.*, 1998a] and the real part of the refractive

index [Yamasoe *et al.*, 1998], were derived. The purpose of this paper is to test a new concept of a consistent method by Dubovik and King (submitted manuscript, 1999) to derive not only the size distribution but also the refractive index and single-scattering albedo. Using rigorous simulations and sensitivity studies, we specify the requirements of the data accuracy to derive these parameters and identify the best combination of measurements in the presence of instrumental errors and particle nonhomogeneity or nonsphericity. For example, we would like to clarify if the simultaneous inversion of the complete data set typically measured by AERONET (sky radiance in the full solar almucantar together with the spectral optical thickness) will always give the best retrievals. Alternatively, we explore if the inversion of sky radiances measured only in the aureole (possibly combined with the spectral optical thickness) can be a preferable retrieval scheme in some situations.

This paper also attempts a comprehensive analysis of possible errors in the aerosol optical characteristics obtained by inversion of AERONET measured radiances. The studies are focused on considering the retrieval accuracy of aerosol parameters (size distribution, refractive index, and single-scattering albedo), which are derived by the inversion algorithm of Dubovik and King (submitted manuscript, 1999) from the typical AERONET measurements of direct and diffuse radiation. The retrieval algorithm is currently being employed for operational use by the AERONET project. The results of the practical retrievals can be found in recent papers [Eck *et al.*, 1999; Smimov *et al.*, 2000b; Dubovik and King, submitted manuscript, 1999] and on the AERONET project web page (<http://aeronet.gsfc.nasa.gov:8080>). In addition, we anticipate that the sensitivity analysis will outline the level of information content of the Sun-sky radiances regarding the aerosol characteristics to be retrieved. Indeed, if the set of measured radiances is not sufficiently informative, the accuracy of the inversions may not be good even if the accuracy of radiance measurements is very high.

2. Sources of Uncertainties and Structure of Error Analysis

The error analysis identifies sources of uncertainties and defines the real accuracy that can be expected for aerosol retrievals from AERONET-measured Sun-sky radiances. Second, the error analysis shows what kind of errors cause the strongest loss of information and strategies for reducing negative effects of these errors on retrieval by optimizing the inversion procedure and selecting the most reliable data. Such selection procedures may optimize measurement geometry, spectral range, choice of a priori information, etc.

2.1. Forward Modeling of Radiances

In order to provide microstructure information from radiance measurements the radiative transfer characteristics of the atmosphere are modeled in the retrieval algorithms [cf. King *et al.*, 1978; Nakajima *et al.*, 1983, 1996] under the assumption of aerosol particles as homogeneous spheres with complex refractive index $\tilde{m}(\lambda)$. The optical data obtained by a ground-based Sun-sky photometer can formally be represented via aerosol microphysical characteristics as follows:

$$\tau^*(\lambda) = \tau[\partial V/\partial \ln r; \tilde{m}(\lambda)] + \Delta_\tau(\lambda) \quad (1)$$

$$I^*(\Theta; \lambda) = I[\partial V/\partial \ln r; \tilde{m}(\lambda); A(\lambda)] + \Delta(\lambda; \Theta),$$

where $\tau(\lambda)$ is the optical depth measured at different wavelengths λ ; $I(\lambda; \Theta)$ is the spectral sky radiance measured at different wavelengths λ and different scattering angles Θ . The asterisk denotes the data known with some uncertainties $\Delta_{s_k}(\cdot)$. The inversion code (Dubovik and King, submitted manuscript, 1999) employed for the current sensitivity studies uses the columnar volume size distribution $\partial V/\partial \ln r$ (for radii from 0.03 to 15 μm) and spectrally dependent complex refractive index $\tilde{m}(\lambda) = n(\lambda) + ik(\lambda)$ as the characteristics to be retrieved. Slight gas absorption for ozone is accounted for from climatological data [see Holben *et al.*, 1998]. All simulations and analysis in this paper are implemented for cloud-free conditions. For the AERONET database these conditions are assured by a cloud-screening algorithm [Smirnov *et al.*, 2000a] considering optical thickness measurements. In addition, the symmetry of the sky radiances in the solar almucantar measured in the right and left hemispheres is checked. The variability of sky radiance due to spectral ground reflectance $A(\lambda)$ is accounted for in a Lambertian approximation with ground reflectance values assumed a priori. The effects of multiple scattering in simulating sky radiance $I(\lambda; \Theta)$ are modeled by the discrete ordinates radiative transfer code for a plane-parallel atmosphere. Two independent discrete ordinates codes by Nakajima and Tanaka [1988] and Stamnes *et al.* [1988] have been used, and both codes have shown equally good performance. Nevertheless, using the truncation approximation of Nakajima and Tanaka [1988] allows for faster calculation of downwelling radiance in the aureole angular range.

2.2. Inversion Scheme

The presence of random errors in the initial measurements data is inevitable. Therefore the optimization of the retrieval methods accounting for the presence of random error is usually highly desirable. The basic concept, methods, and procedures of such optimization are widely discussed and developed by the theory of statistical estimation [cf. Edie *et al.*, 1971]. Nevertheless, the efficient implementation of statistical optimization for the purposes of practical inversion is a rather challenging task. The discussion of employing statistical optimization for the atmospheric optics applications can be found, for example, in the papers by Rodgers [1976] and Dubovik *et al.* [1995a, 1998b]. The details of designing statistically optimized code for atmospheric aerosol retrieval from Sun-sky radiances are given by Dubovik and King (submitted manuscript, 1999). According to the chosen inversion strategy, the results are derived from the complex data set, which includes both the measurements of a Sun-sky photometer and a priori data constraining the retrieved results. Therefore the retrieved aerosol optical characteristics should satisfy simultaneously both the measured radiances united in (1) and the system of a priori defined constraints:

$$\begin{aligned} s_1^*(r) &= s_1(dV/d \ln r) + \Delta_{s_1}(r) \\ s_2^*(\lambda) &= s_2[n(\lambda)] + \Delta_{s_2}(\lambda) \\ s_3^*(\lambda) &= s_3[k(\lambda)] + \Delta_{s_3}(\lambda), \end{aligned} \quad (2)$$

where the values $s_k(\cdot)$ relate to a priori assumed values defining the smoothness of the retrieved characteristics. For smoothing the solution the norm of the m th logarithmic derivatives of the retrieved characteristics $f(x)$ are restricted:

$$\begin{aligned} a_m &= \int \left(\frac{d^m \ln f(x)}{d^m x} \right)^2 dx \approx \sum_{j=1}^n \left(\frac{\Delta^m \ln f(x)}{(\Delta x)^m} \right)^2 \Delta x \\ &= (\Delta x)^{-2m+1} \mathbf{x}^T (\mathbf{S}_m)^T (\mathbf{S}_m) \mathbf{x}, \end{aligned} \quad (3)$$

where $\Delta^m(x_j)$ is the m th difference, \mathbf{S}_m contains the coefficients for calculating m th differences, and T denotes matrix transposition. The application of such smoothing to stabilize the inversion has been proposed by Phillips [1962], Twomey [1963], and Tikhonov [1963], and it is commonly used in atmospheric aerosol retrievals [cf. King *et al.*, 1978; Nakajima *et al.*, 1983]. The difference with the approach of the abovementioned papers is that we are restricting the logarithmic derivatives following Dubovik *et al.* [1995a] rather than restricting the absolute derivatives. Also, we are restricting several functions simultaneously ($dV/d \ln r$, $n(\lambda)$, and $k(\lambda)$), and for each function we constrain different values a_m ($m = 1, 2, 3$). That is, the admissible variations for the size distribution $\partial V/\partial \ln r(r)$ are expected to be much stronger than for spectral variations of the real $n(\lambda)$ and imaginary $k(\lambda)$ parts of the refractive index. This is why we are considering derivatives of higher order for $dV/d \ln r$ and only first and second derivatives for $n(\lambda)$ and $k(\lambda)$. Besides, a priori values of a_m are much less for $n(\lambda)$ and $k(\lambda)$ than for $dV/d \ln r$.

The inversion is designed as a search for the best fit of all considered data by a theoretical model taking into account the different levels of accuracy of the fitted data in a manner similar to Dubovik *et al.* [1995a]. This design provides the most accurate solution (the smallest variances of the retrieval errors) in the presence of random noise. The optimized solution corresponds to the minimum of the quadratic form:

$$\Psi(\mathbf{a}) = \sum_{k=1}^5 \gamma_k \{ [\mathbf{f}_k^* - \mathbf{f}_k(\mathbf{a})]^T (\mathbf{W}_k)^{-1} [\mathbf{f}_k^* - \mathbf{f}_k(\mathbf{a})] \}, \quad (4)$$

where the vector \mathbf{f}_1 corresponds to the logarithms of $\tau(\lambda)$ at the selected wavelengths, the vector \mathbf{f}_2 corresponds to the logarithms of $I(\lambda; \Theta)$ at the selected wavelengths and angles, the vector \mathbf{f}_3 includes the values of size distribution smoothing function in the grid points r_i , and \mathbf{f}_4 and \mathbf{f}_5 include the values of $n(\lambda)$ and $k(\lambda)$ smoothing functions. The matrices \mathbf{W}_k are the weight matrices of random errors in the input data sets. The vector \mathbf{a} includes the logarithms of the retrieved values of the size distribution $dV/d \ln r(r_i)$ in the grid points and the values of real and imaginary parts of the refractive index $n(\lambda_i)$ and $k(\lambda_i)$ at the selected wavelengths. The Lagrange coefficients γ_k are defined from statistical consideration as the ratios of the error variances Δ_k : $\gamma_k = \varepsilon_1^2/\varepsilon_k^2$. It should be noted that the smoothness restrictions are used only for the purpose of avoiding unrealistic oscillations. The correspondent variances ε_m^2 are defined as $\varepsilon_m^2 = \langle a_m \rangle (\Delta r)^{2m+1}$, where a_m is the maximum value observed for climatologically known aerosol characteristics. The multivariable search for the minimum of (4) is implemented by a stable numerical procedure combining matrix inversion and univariant relaxation according to Dubovik *et al.* [1998b].

2.3. Random Errors

The effect of expected random errors is incorporated in the inversion procedure by Dubovik and King (submitted manuscript, 1999), as is briefly described in section 2.2. Correspondingly, the expected random errors of the retrieval can be esti-

Table 1. Spectral and Angular Characteristics of AERONET Sun/Sky Radiance Data Used for Sensitivity Tests

Angular and Spectral Characteristics	Measurements and Assumptions
Wavelengths Sun and sky radiance measurements, nm	440, 670, 870, and 1020
Azimuth angle relative to Sun ϕ_j (standard sky radiance almucantar taken by AERONET), deg	2, 2.5, 3, 3.5, 4, 5, 6, 10, 12, 14, 16, 18, 20, 25, 30, 35, 40, 45, 50, 60, 70, 80, 90, 100, 120, 140, 160, and 180
Scattering angle Θ_j (solar almucantar for solar zenith angle $\theta_0 = 60^\circ$), deg	1.73, 2.2, 2.60, 3.1, 3.46, 4.33, 5.20, 8.66, 10.39, 12.12, 13.85, 15.57, 17.30, 21.61, 25.90, 30.19, 34.46, 38.71, 42.94, 51.32, 59.57, 67.65, 75.52, 83.12, 97.18, 108.94, 117.05, and 120.00
Spectral values of ground reflectance $A(\lambda)$ (a green vegetation model)	$A(440 \text{ nm}) = 0.03$; $A(670 \text{ nm}) = 0.06$; $A(870 \text{ nm}) = 0.2$; and $A(1020 \text{ nm}) = 0.2$
Spectral values of ground reflectance $A(\lambda)$ (a bare soil model)	$A(440 \text{ nm}) = 0.07$; $A(670 \text{ nm}) = 0.15$; $A(870 \text{ nm}) = 0.25$; and $A(1020 \text{ nm}) = 0.25$

mated and controlled by the means of estimation theory formulations. For this retrieval the covariance matrix of retrieval errors caused by random noise can be estimated by the expression

$$\mathbf{C}_{\hat{\mathbf{a}}} = \left(\sum_{k=1}^5 \gamma_k (\mathbf{U}_{k,\hat{\mathbf{a}}})^T (\mathbf{W}_k)^{-1} (\mathbf{U}_{k,\hat{\mathbf{a}}}) \right)^{-1} \hat{\boldsymbol{\varepsilon}}_1^2, \quad (5)$$

where $\mathbf{U}_{i,\hat{\mathbf{a}}}$ is the Jacobi matrix of the first derivatives in the near vicinity of the solution, i.e.,

$$\{\mathbf{U}_{k,\hat{\mathbf{a}}}\}_{ji} = \left. \frac{\partial \{[\mathbf{f}_k(\mathbf{a})]\}_j}{\partial a_i} \right|_{\hat{\mathbf{a}}}.$$

The value of variance $\hat{\boldsymbol{\varepsilon}}_1^2$ is estimated from the value of the residual (i.e., from the obtained minimum of the quadratic form $\Psi(\mathbf{a})$). This residual, in the case of normal noise, has a χ^2 distribution. Correspondingly, the variance $\hat{\boldsymbol{\varepsilon}}_1^2$ can be estimated from the residual as follows:

$$\hat{\boldsymbol{\varepsilon}}_1^2 \approx \Psi_{\min}(\mathbf{a}) / (M - N), \quad (6)$$

where M is the number of fitted Sun-sky radiances and a priori data in a single inversion and N is the number of retrieved parameters.

Thus estimates of the retrieval errors due to random noise are given by (5) and (6). These equations were derived in the approximation of linear dependence errors of the retrieval from errors of measurements. In practice, we find that these formulations work quite well in the case of small values of $\hat{\boldsymbol{\varepsilon}}_1^2$. In cases of moderate and large values of $\hat{\boldsymbol{\varepsilon}}_1^2$, (5) and (6) tend to overestimate the retrieval errors; that is, they give an upper limit to the expected errors.

2.4. Systematic Errors

Systematic errors mainly occur because of the following two reasons: the existence of unaccounted instrumental problems (offsets) during the actual registration of Sun-sky radiance or the use of invalid approximations in the theoretical model used for measurement interpretation. These errors coupled with the random errors result in simultaneous overestimating or under-

estimating optical depth, sky radiances, or azimuth pointing angle. These uncertainties can be very different from random noise uncertainties because the change in measured Sun-sky radiance caused by systematic offsets (such as simultaneous overestimation or underestimation of optical depth, sky radiance, azimuth pointing angle, etc.) may look rather similar to the change caused by some real variation of optical properties of the atmospheric aerosol. Correspondingly, the effect of this kind of systematic error on the aerosol retrievals may not be estimated correctly by (5) and (6), and we analyze the retrieval errors caused by systematic errors separately.

Selecting data that are the most reliable for the inversion can reduce the effect of systematic errors on the retrieval. Such selection may relate to optimizing the measurement geometry (e.g., measurements of sky radiances can be restricted to only the aureole angular range), spectral range, etc., where the radiances are less likely affected by the unaccounted instrumental problems and the retrievals less sensitive to the approximations in forward modeling. Therefore our error analysis will address this aspect of the inversion as well.

3. Error Analysis

The algorithm has been applied for simultaneous retrieval of the volume size distribution $dV/d \ln r(r)$, complex refractive index, and single-scattering albedo $\omega_0(\lambda)$ from the basic set of Sun-sky radiance set measured in the solar almucantar by AERONET Sun-sky radiometers. Correspondingly, in our sensitivity studies we are analyzing the errors in retrieval of $dV/d \ln r(r)$, $n(\lambda)$, $k(\lambda)$, and $\omega_0(\lambda)$, which characterize the typical aerosol retrieval parameters of AERONET.

For the inversion input, Sun radiance and angular distribution of sky radiance in the solar almucantar ($\theta_0 = \theta$, where θ_0 is the solar zenith angle and θ is the zenith angle of observations) are used. Azimuth angles of the observations ϕ_j are given in Table 1. Both Sun and sky radiances are taken spectrally at four wavelengths (Table 1). This is the basic data set that is collected routinely by AERONET Sun-sky radiometers according to established measurements protocol [Holben *et al.*, 1998]. Six sky radiance scans in the solar almucantar are measured daily at an optical airmass m_0 ($m_0 \approx 1/\cos(\theta_0)$ for $\theta_0 \leq 75^\circ$) of 4, 3, and 2, both morning and afternoon, and a sky almucantar scan is measured hourly between $m_0 = 2$ in the morning and afternoon. The solar zenith angle $\theta_0 = 60^\circ$ has been chosen for our sensitivity tests because the solar almucantar with $\theta_0 = 60^\circ$ has a rather wide angular coverage of sky radiance. The scattering angles Θ_j corresponding to sky radiance in such an almucantar correspond to the scattering angles Θ_j presented in Table 1 (Θ_j for the almucantar is related to azimuth observation angles ϕ_j by the simple geometrical formulation $\cos(\Theta_j) = \cos^2(\theta_0) + \sin^2(\theta_0) \cos(\phi_j)$). The scattering angle $\Theta = 120^\circ$ is of particular importance because this is the typical angular range of many sunsynchronous satellites. The random errors are estimated by (5) and (6) as explained in section 2.3. The retrieval errors caused by a particular instrumental offset are analyzed by means of the following straightforward numerical test. First, for the chosen aerosol model, Sun and sky radiances are computed for an "error-free" condition (this condition is discussed below). Afterward, the offset is included in the simulated radiances, and these radiances are inverted. The comparison of the inversion result obtained with the assumed aerosol characteristic shows the retrieval error. Similarly, the errors caused by approxima-

Table 2. The Aerosol Models Adapted for Numerical Sensitivity Tests

Aerosol Type	σ_1	σ_2	r_{V1}	r_{V2}	C_{V1}/C_{V2}	r_{N1}	r_{N2}	C_{N1}/C_{N2}	$n(\lambda)$	$k(\lambda)$	$\tau(440)$
Water-soluble	0.6	0.6	0.118	1.17	2	0.04	0.4	2,000	1.45	0.0035	0.05
											0.20
											0.50
											1.00
Dust 1	0.6	0.8	0.1	3.4	0.066	0.034	0.5	735	1.53	0.008	0.50
Dust 2	0.6	0.6	0.1	1.17	0.066	0.034	0.4	107	1.53	0.008	1.00
Biomass Burning	0.4	0.6	0.132	4.5	4	0.082	1.52	65,700	1.52	0.025	0.50
											1.00

tions in modeling are considered. That is, the Sun and sky radiances are simulated by the most accurate available model, which does not use the approximation being tested. Then, these simulated radiances are inverted by the code, which utilizes the tested approximation in the modeling. The differences between retrieved and assumed values of aerosol characteristics give the apparent errors of the retrieval.

Obviously, both the effect of random and systematic errors may be different for different kinds of aerosol because the relationships between inverted and retrieved characteristics are nonlinear. Therefore the error analysis is applied to three significantly different aerosol models. The optical model (the shape of size distribution and the values of complex refractive indices) of water-soluble aerosol and dust are utilized from the paper of *Tanré et al.* [1999]. The biomass-burning aerosol is modeled according to *Remer et al.* [1998]. According to these papers, particle volume size distribution is modeled by bimodal lognormal size distribution as follows:

$$\frac{dR^n(r)}{d \ln r} = \sum_{i=1}^2 \frac{C_{n,i}}{\sqrt{2\pi}\sigma_i} \exp \left[-\frac{1}{2} \left(\frac{\ln r - \ln r_{n,i}}{\sigma_i} \right)^2 \right],$$

where index n refers to the kind of size distribution (e.g., $dR^0(r)/d \ln r = dN(r)/d \ln r$ and $dR^3(r)/d \ln r = dV(r)/d \ln r$), index i denotes fine ($i = 1$) and coarse ($i = 2$) modes of aerosol, C denotes particle concentration ($C_{0,i} = C_{Ni}$ for number distribution and $C_{3,i} = C_{Vi}$ for volume distribution), $r_{n,i}$ denotes median radius ($r_{0,i} = r_{Ni}$ for number distribution and $r_{3,i} = r_{Vi}$ for volume distribution), and σ_i is the standard deviation. The values for particle volume size distributions (and corresponding particle number size distribution) and complex refractive indices are displayed in Table 2. For the case of the water-soluble aerosol both clear and hazy conditions are considered. The values of optical thickness are also given in Table 2. Dust and biomass-burning aerosols are usually a consequence of such phenomena as dust storms or extensive fires, and correspondingly, these aerosols are often characterized by relatively high optical thickness. Therefore, in the numerical tests we consider only optical situations with high aerosol loading. The spectral values (Table 1) of ground albedo were defined for water-soluble aerosol and dust according to a green vegetation model. For biomass-burning aerosol the ground reflectance of bare soil was assumed (Table 1). Spectral bidirectional reflectances of a bare soil site and vegetation sites of differing densities are given by *Deering* [1989] and *Soulen et al.* [2000], and for forested sites they are given by *Ranson et al.* [1994] and *Tsay et al.* [1998].

3.1. Algorithm Performance in Error-Free Conditions

The error-free condition is used here to note that neither systematic nor random errors were specifically introduced ei-

ther in the forward simulations or in the inversion algorithm. However, it should be noted that some minor errors are always present in the radiance modeling used for inversion. These errors are inherent to the inversion algorithm. First, in the numerical inversion used, all retrieved analytical functions are represented by a limited number of parameters; that is, some approximations are always used. For example, the aerosol optical characteristics (phase function ($P(\Theta)$), extinction, scattering, and absorption optical thickness ($\tau_{\text{ext}}(\lambda)$, $\tau_{\text{scat}}(\lambda)$, and $\tau_{\text{abs}}(\lambda)$) are modeled from microstructure parameters ($dV/d \ln r$, $n(\lambda)$, and $k(\lambda)$) using the following approximations:

$$\begin{aligned} \tau_{\tau_i}(\lambda) &= \left(\frac{2\pi}{\lambda} \right) \int_{r_{\min}}^{r_{\max}} K_{\tau_i}(\lambda; n; k; r) \frac{dV}{d \ln r} d \ln r \\ &\approx \mathbf{K}_{\tau_i}(\lambda; n; k) \mathbf{v} \end{aligned} \quad (7)$$

$$\begin{aligned} \tau_{\text{scat}}(\lambda) P(\Theta) &= \left(\frac{2\pi}{\lambda} \right) \int_{r_{\min}}^{r_{\max}} K_{\text{scat}}(\Theta; \lambda; n; k; r) \frac{dV}{d \ln r} d \ln r \\ &\approx \mathbf{K}_{\text{scat}}(\Theta; \lambda; n; k) \mathbf{v}, \end{aligned} \quad (8)$$

where the kernel functions of optical thickness $K_{\tau_i}(\cdot)$ and differential scattering coefficient $K_{\text{scat}}(\cdot)$ are approximated by matrices $\mathbf{K}_{\tau_i}(\cdot)$ and $\mathbf{K}_{\text{scat}}(\cdot)$. The volume size distribution $dV(r)/d \ln r$ is approximated by the vector \mathbf{v} with 22 elements corresponding to the points $\{\mathbf{v}\}_i = dV(r_i)/d \ln r$ chosen with equal steps $\Delta \ln r = \ln r_{i+1} - \ln r_i = \text{constant}$. The trapezoidal approximation [*Twomey*, 1977] is used to obtain size distribution values between these r_i points in the matrices $\mathbf{K}_{\tau_i}(\cdot)$ and $\mathbf{K}_{\text{scat}}(\cdot)$ calculation. Also, to meet calculation speed requirements, the dependence of matrices $\mathbf{K}_{\tau_i}(\cdot)$ and $\mathbf{K}_{\text{scat}}(\cdot)$ on real n and imaginary m part of refractive index are approximated from look-up tables over all possible n and k value (see *Dubovik and King* (submitted manuscript, 1999) for further details).

All of the abovementioned approximations produce some error even in so-called error-free conditions. According to our estimations, these errors can be considered as relative random errors with standard deviation $<1\%$ for all three considered aerosol models. For significantly narrower size distributions (which are rather unlikely for atmospheric aerosols) this error may increase to up to 2–3%. Such an accuracy of the algorithm is sufficient for AERONET applications because the random error of the measurements, which is at the level of 3–5%, dominates over the uncertainty of the optical characteristics modeling.

Thus the performance of the algorithm in error-free conditions shows the stability of the inversion to minor random errors. It should be noted that the problem of simultaneous retrieval of the complex refractive index together with the size

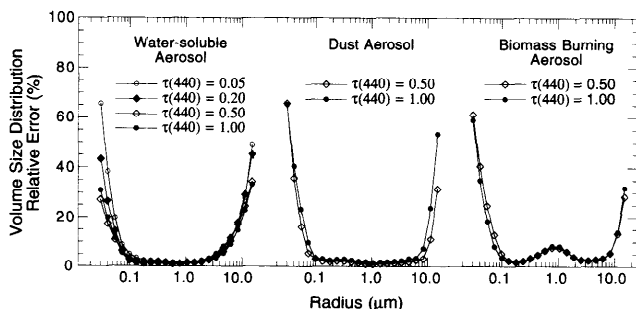


Figure 1. The standard deviation of the errors in estimates of volume size distribution caused by random errors.

distribution in an extended range of sizes (0.03–15 μm) belongs to the class of so-called ill-posed inverse problems. For example, implementing an inversion of Sun-sky radiances without applying any a priori constraints (i.e., $\gamma_k = 0$ for $k = 3, 4, 5$ in (2)) gives rather unstable and nonunique results (the illustrations are given by Dubovik and King (submitted manuscript, 1999)). Therefore it is important to illustrate performance and discuss the retrieval accuracy of the algorithm in the error-free condition. The retrieval accuracy in error-free conditions can be considered as the maximum possible accuracy that can be achieved by the inversion algorithm.

The errors existing in error-free conditions could be considered as random errors, and correspondingly, the retrieval errors can be estimated following (5) and (6). To increase the confidence in these approximated formulations, we produced a series of numerical tests in error-free conditions for all three selected aerosol models. The results agree well with estimations by (5) and (6). Thus the standard deviations of the retrieval error in error-free conditions can be expected as follows: 0.01 for $n(\lambda)$, 10% for $k(\lambda)$, and 0.01 for $\omega_0(\lambda)$. The errors in the retrieved size distribution $dV(r)/d \ln r$ is a function of particle size. Figure 1 illustrates the size distribution error standard deviations estimated according to (5) and (6) for three different aerosol microphysical models. It can be seen that the errors significantly increase for both small sizes ($r < 0.1 \mu\text{m}$) and large sizes ($r > 7 \mu\text{m}$). For example, Figure 2 shows retrieval results obtained by numerical tests for bimodal aerosol size distribution that have particles in the whole considered particle size range. According to the results of the tests, Figure 2 shows the accuracy limit for the size distribution retrieval: Fine particles with a mode radius $< 0.05 \mu\text{m}$ for the smallest mode and large particles with a mode radius $> 10 \mu\text{m}$ for the largest mode cannot be retrieved with an acceptable accuracy even in error-free conditions. The increase of the errors for both cases of very small and very large particles can be explained by the fact that the contribution of these particles to the measured optical characteristics is significantly smaller than for particles of intermediate sizes ($0.1 \mu\text{m} < r < 7 \mu\text{m}$).

3.2. Offsets

The offsets in the AERONET radiance measurements can be caused by miscalibrations of the radiometer Sun-sky channels or by possible temporary loss in precision and/or accuracy of angle pointing. The appearance of such offsets generates systematic errors in the two first data sets of the equation system (1). That is, the possible offset in the solar channel calibration is expected to generate a wavelength-independent absolute uncertainty in $\tau(\lambda)$ at the level of ± 0.01 [Holben et al.,

1998]. An integrating sphere is utilized to perform the sky channel calibrations, and the expected accuracy of this calibration is $\sim 5\%$ or better [Holben et al., 1998]. Therefore the possible offsets in sky radiance registration should not exceed 5%. The mechanical degradation of the robot, which points the radiometer, may result in degraded precision in directional pointing. We estimate pointing accuracy to be within 0.05° (one motor step interval) for a well-tuned instrument and $\sim 0.25^\circ$ (or 0.5° – 1.0° in the worst case scenario) for a degraded or improperly aligned instrument.

Also, the error in assumed ground albedo can be considered as an additional offset (not an instrumental offset). Indeed, the ground reflectance is incorporated in the scattering model by assuming Lambertian reflectance (independent of scattering angle) with reflectance values a priori fixed at each wavelength. It is expected that such an assumption is sufficient for the interpretation of ground-based atmospheric measurements because the reflected light is of second-order importance for the downward radiation in most situations. The a priori fixed reflectance introduces some uncertainty in the retrievals. We consider simultaneous overestimation or underestimation of ground reflectance in the whole spectrum to be the most probable scenario of this kind of uncertainty.

Errors in the measured Sun-sky radiances caused by offsets can be significantly different from random errors. This difference can be especially distinct for a single retrieval where there is no averaging of any of the abovementioned offsets. Indeed, for a single almucantar data set the spectral optical depth and/or angular distribution of sky radiances and/or angle pointing and/or a priori estimates of ground reflectance can be systematically shifted. At the same time, for long-term measurements of aerosol in similar conditions, errors due to offsets can be significantly averaged and therefore reduced. Such averaging is expected because of the maintenance procedures being performed during the averaging period. The instruments are calibrated, checked, adjusted, or replaced; details are given by Holben et al. [1998] who establishes procedures for maintaining the quality of the measurements. Unfortunately, the systematic presence of similar error in the a priori estimates of ground reflectance is likely even for long-term measurements because currently there is no reliable procedure for determining spectral ground reflectance values. In future analysis and subsequent reprocessing of AERONET data sets we plan to utilize the global database of surface spectral bidirectional reflectance and spectral albedo that will be produced from analysis of the Moderate-Resolution Imaging Spectrometer

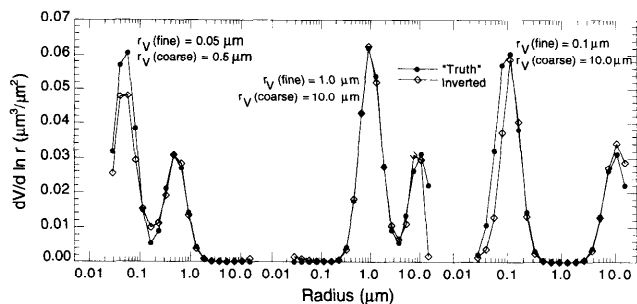


Figure 2. The results of size distribution retrievals in “error-free” conditions. The different combinations of mode radii of coarse and fine particles are considered. The complex refractive index is assumed same as for water-soluble aerosol model.

(MODIS) instrument data on the Terra (formerly known as EOS AM) and EOS PM satellites. Therefore we expect that the magnitude of the systematic error in assumed ground reflectance will be minimized when using these data sets and will be lower than the values of 30 and 50% relative errors used in the analysis presented here.

All or some of the above shifts occurring simultaneously (in the optical depth, sky radiance, angle pointing, and ground reflectance) are very unlikely and would probably mean that the data would be unacceptable for interpretation. The simultaneous uncorrected appearance of several minor shifts is possible, but this would happen randomly and can be analyzed as random errors. In our opinion, the most serious problem that may appear in practice would be the appearance of one of above-mentioned offsets. Therefore, in our tests we will analyze each situation with a single but strong offset.

3.2.1. Offsets modeling. Instrumental offsets are considered in our analysis as the three following systematic errors: (1) wavelength-independent absolute shifts in the measured total optical thickness $\tau(\lambda)$, $\Delta\tau(\lambda) = \pm 0.01$ and $\Delta\tau(\lambda) = \pm 0.02$ (as a maximum possible shift in the measured total optical thickness); (2) wavelength-independent relative shifts in the measured sky radiances $I(\Theta; \lambda)$, $\Delta I(\Theta; \lambda)/I(\Theta; \lambda)$ 100% = $\pm 5\%$; and (3) systematic shifts in the azimuth angle pointing, $\Delta\phi = 0.5^\circ$ and $\Delta\phi = 1^\circ$ (as a maximum possible shift in angle pointing). Errors in priori estimates of ground albedo values $A(\lambda)$ are modeled as wavelength-independent relative shifts in a priori assumed ground albedo values $A(\lambda)$, $\Delta A(\lambda)/A(\lambda)$ 100% = $\pm 30\%$, $\pm 50\%$.

The above errors do not exhaust all error sources affecting Sun-sky radiance measurements. At the same time, according to the multiyear experience of processing and analyzing the network data, these errors adequately reflect all major practical problems of AERONET instrumentation. For example, extinction optical thickness error is the result of multiple sources of error [Shaw, 1976; Reagan et al., 1986; Russell et al., 1993] and probably cannot be reduced to a wavelength-independent absolute shift $\Delta\tau(\lambda) = \pm 0.01$. However, for AERONET radiometer measurements the uncertainty in direct Sun measurements is dominated by the calibration uncertainty in exoatmospheric constant determined by Langley plot procedure and in the change in time of these exoatmospheric constants due to change in interference filter transmittance.

3.2.2. Result of numerical tests. The results of numerical tests for aerosol retrievals in the presence of the various offsets described above are presented in Figures 3–7. Figures 3 and 4 show the retrievals of aerosol size distribution and optical properties for water-soluble aerosol and for different values of aerosol optical thickness ($\tau(440) = 0.05, 0.2, 0.5$, and 1). The results for the retrievals of desert dust-type aerosol and biomass-burning aerosol are presented in Figures 5–7.

3.2.2.1. Size distributions: The size distributions can be retrieved rather well in almost all situations considered (compare Figures 3, 5, and 6). The major concerns relate to the characterization of water-soluble aerosol in optically thin conditions: $\tau(440) = 0.05$ and 0.2 and retrievals of the size distribution of dust when angular pointing is offset. In optically thin situations the largest retrieval errors result from biases in optical thickness. This is because even a small absolute error in optical thickness $\Delta\tau(\lambda) = \pm 0.01$ becomes comparable with the magnitude of aerosol optical thickness and produces a very high relative error $\Delta\tau(\lambda)/\tau(\lambda)$ (20% and higher). In optically thin situations a certain increase in the retrieval errors is noted

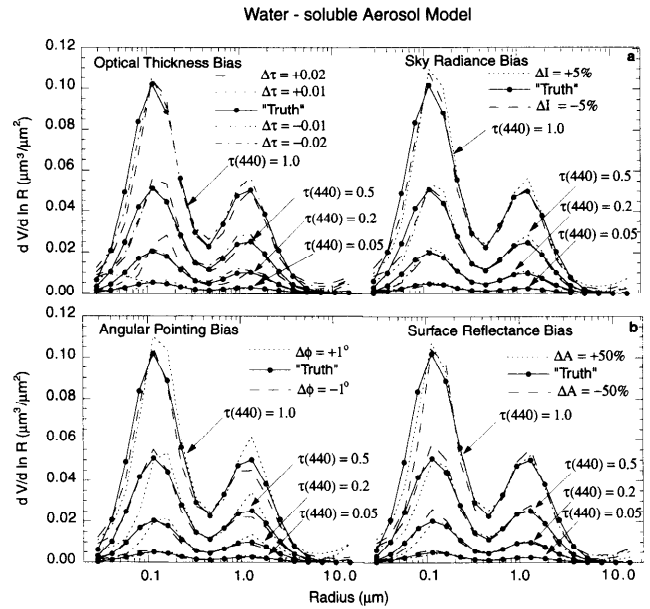


Figure 3. Volume size distribution retrievals for water-soluble aerosol in the presence of instrumental offsets: (a) biases in optical thickness (left) and sky radiances (right) and (b) biases in angular pointing (left) and a priori estimates of ground reflectance (right).

for all of the offsets considered. This increase can be explained by the fact that the contribution of the atmospheric aerosol to both Sun and sky radiances becomes comparable or even smaller than contributions from molecular scattering and gaseous absorption.

The high sensitivity of dust size distribution to errors in angular pointing can also be easily understood. That is, the aureole part of the phase function ($\Theta < 40^\circ$) is very sensitive to large particles, and hence significant information about large particles ($r \gg \lambda/2\pi$) is concentrated in the small-angle scattering range [e.g., Bohren and Huffman, 1983]. In addition, the phase function of large particles has a very well pronounced forward peak ($P^{\text{act}}(\Theta)$ at a scattering angle of 0° can be >10 times greater than at a scattering angle of 10°). The contribution of multiple scattering in the aureole is also very minor [cf. Dave, 1964; Nakajima et al., 1996]. Thus a small error in angular pointing for the scattering by dust particles, which are accounted by large coarse mode particles, leads to a very significant error in the sky radiances measured in the aureole range and correspondingly to a very significant error in the retrieved size distribution. A similar tendency can be observed in the retrieval of the coarse particles mode of the biomass-burning aerosols (Figure 6).

3.2.2.2. Complex refractive index and single-scattering albedo: The complex refractive index and single-scattering albedo are optical characteristics of great interest for the various aerosol studies, and much effort has been expended to achieve reliable retrievals of these characteristics from optical measurements. However, many of these studies have not yet resulted in well established and reliable procedures. In our opinion, the reason for such modest progress in the development of retrieval procedures relates to the limited information content of optical measurements with respect to complex refractive index and single-scattering albedo. The numerical tests clearly

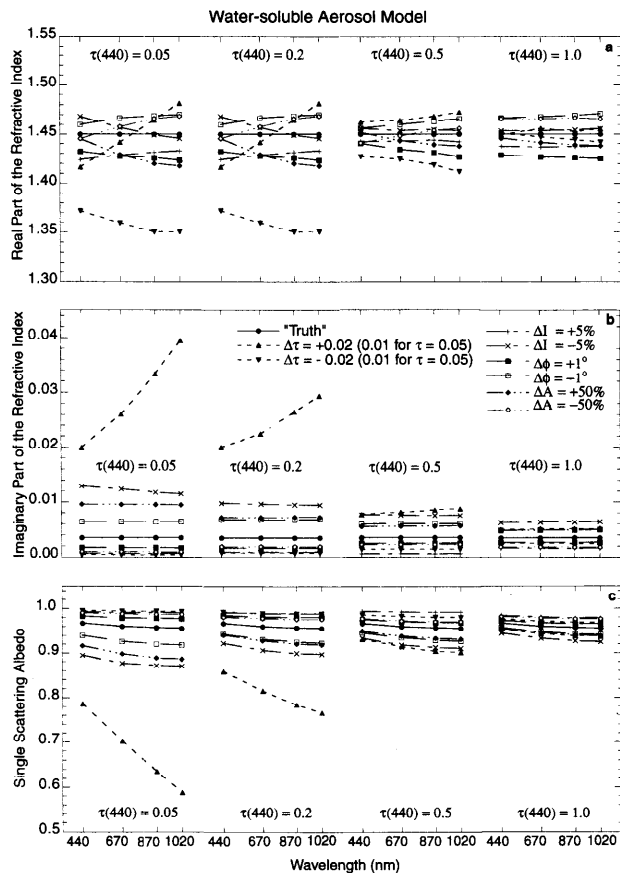


Figure 4. Complex refractive index and single-scattering albedo retrievals in the presence of instrumental offsets for water-soluble aerosol: (a) the real part of the complex refractive index, (b) the imaginary part of the complex refractive index, and (c) the aerosol single-scattering albedo.

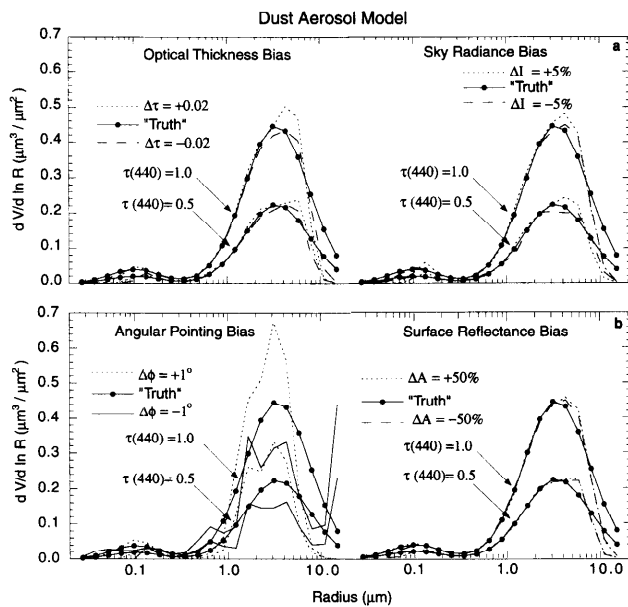


Figure 5. Volume size distribution retrievals for desert dust in the presence of instrumental offsets: (a) biases in optical thickness (left) and sky radiances (right) and (b) biases in angular pointing (left) and a priori estimates of ground reflectance (right).

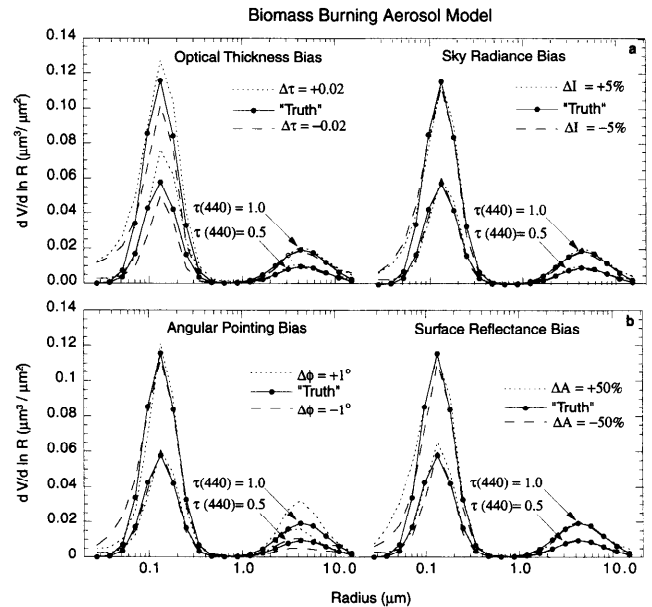


Figure 6. Volume size distribution retrievals for biomass-burning aerosol in the presence of instrumental offsets: (a) biases in optical thickness (left) and sky radiances (right) and (b) biases in angular pointing (left) and a priori estimates of ground reflectance (right).

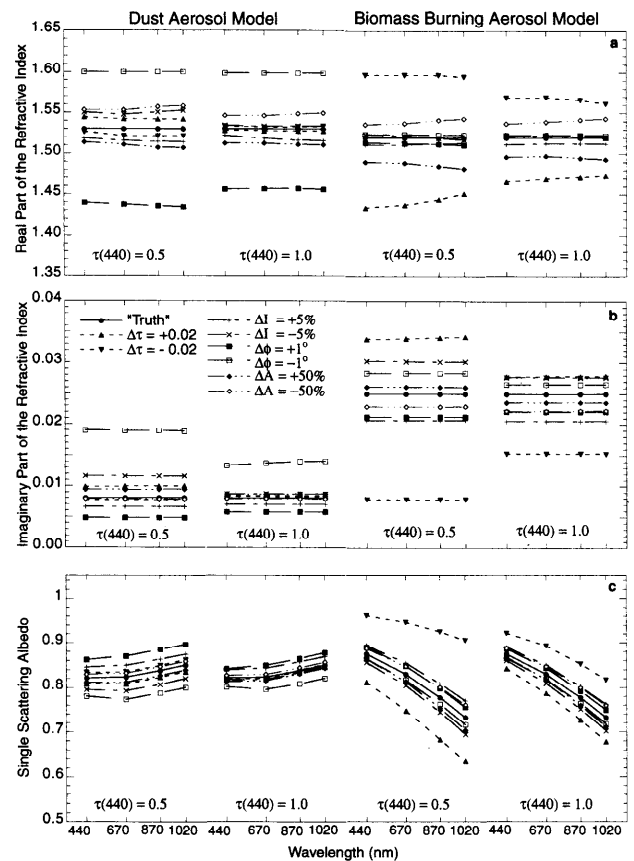


Figure 7. Complex refractive index and single-scattering albedo retrievals in the presence of instrumental offsets for desert dust and biomass-burning aerosol: (a) the real part of the complex refractive index, (b) the imaginary part of the complex refractive index, and (c) the aerosol single-scattering albedo.

show these accuracy limitations of Figures 4 and 7. Indeed, the applied inversion code allows global fitting of spectral and multiangle Sun-sky radiance with a simultaneous search for the size distribution and complex refractive index. Testing this code in error-free conditions shows a successful retrieval of all searched parameters. However, in the presence of offsets the accuracy of the retrieval significantly degrades, particularly for the retrieval of the complex refractive index and single-scattering albedo. For example, the tendency of increasing retrieval errors with a decrease of optical thickness is more pronounced for the retrieval of the refractive index and single-scattering albedo (Figures 4 and 7) than for the retrieval of aerosol size distribution. The retrieval accuracy of each of above parameters (real part of refractive index and imaginary part of refractive index and single scattering albedo) is discussed in detail below.

3.2.2.3. Real part of the refractive index: The real part of the refractive index of water-soluble aerosol is retrieved sufficiently well only for the cases with high optical thickness: $\tau(440) = 0.5$ and 1 (Figure 4). For optically thin conditions ($\tau(440) = 0.05$ and 0.2) the accuracy of the real part of refractive index is significantly reduced. This result arises primarily from the low sensitivity of Sun-sky radiance measurements to aerosol of low concentration (i.e., low optical thickness). It should be noted that the offset in optical thickness (Figure 4, $\tau(440) = 0.05$ and 0.2) results in an artificial wavelength dependence of $n(\lambda)$. This can be explained by the fact that the error in optical thickness measurements is assumed wavelength-independent $\Delta\tau(\lambda) = \pm 0.01$. At the same time, the aerosol optical thickness $\tau^{\text{aer}}(\lambda)$ can be strongly wavelength-dependent, and thus the effect of $\Delta\tau(\lambda)$ can be different (in proportional sense) at different wavelengths. The wavelength dependence of $\tau^{\text{aer}}(\lambda)$ can be characterized by the Ångström parameter α , which is a coefficient of the following regression:

$$\ln[\tau(\lambda)] = -\alpha \ln(\lambda) + \beta. \quad (9)$$

The value of the Ångström exponent α is usually anticorrelated with aerosol microstructure: The smaller the aerosol particles, the higher the α and vice versa [e.g., *O'Neill and Royer, 1993*]. Table 3 shows the Ångström exponents of all the considered aerosols together with wavelength dependence of $\tau^{\text{aer}}(\lambda)$ for the case of $\tau(440) = 0.5$. We see that $\tau^{\text{aer}}(\lambda)$ is very different for the different aerosol types. For the smaller particles we see higher values of α , and hence a stronger wavelength dependence of error effects are expected (we see such dependence for water-soluble aerosol in Figure 4). From Figure 7 we can see that the error effect caused by $\Delta\tau(\lambda)$ is the smallest for dust and much more pronounced for biomass burning. This is because dust has both a small value of α and a large value of τ . The biomass-burning aerosol has a high optical thickness at 440 nm but with a very high value of the Ångström exponent and therefore $\tau^{\text{aer}}(\lambda)$ strongly decreasing with λ .

The largest error in $n(\lambda)$ for the dust model size distribution (Figure 7) arises from angle pointing bias, similar to results for the size distribution retrieval, discussed above. For dust the greatest information about the real part of the refractive index comes from the aureole region, which is strongly affected by errors in angular pointing.

3.2.2.4. Imaginary part of the refractive index: The imaginary part of the refractive index retrievals are illustrated in Figures 4 and 7. The value of imaginary part of refractive index defines the magnitude of the aerosol absorption. Therefore the error in $k(\lambda)$ correlates with the error $\Delta\tau(\lambda)$. That is, an

Table 3. Spectral Aerosol Optical Thickness and Ångström Exponent α for the Aerosol Models Adapted for Numerical Sensitivity Tests

	440 nm	670 nm	870 nm	1020 nm	α
Water-soluble	0.50	0.26	0.18	0.14	1.5
Dust 1	0.50	0.40	0.38	0.37	0.36
Biomass burning	0.50	0.22	0.13	0.08	2.1

increase (decrease) of $\tau^{\text{aer}}(\lambda)$ caused by the presence of the error $\Delta\tau(\lambda)$ is compensated by the inversion code as an artificial increase (decrease) of absorption (i.e., $k(\lambda)$). This effect can be observed in the situations where $\Delta\tau(\lambda)$ is not negligible in comparison with $\tau(\lambda)$, i.e., for water-soluble aerosol (where optical thickness is low, $\tau(440) = 0.05$ and 0.2) and for biomass-burning aerosol ($\tau(\lambda)$ for larger wavelengths is rather small because of high $\alpha = 2.1$). For the dust case the retrieval of $k(\lambda)$ is mainly influenced by error in the angular pointing. This confirms the statement, made previously, that the major information about aerosol parameters for large dust particles arises from aureole radiances, which are very sensitive to the angular pointing accuracy.

3.2.2.5. Single-scattering albedo: Single-scattering albedo retrievals are shown in Figures 4 and 7. All of the observed tendencies of retrieved $\omega_0(\lambda)$ can be anticipated from the following simple formula:

$$\frac{\Delta\omega_0}{\omega_0} \approx \frac{\Delta\tau_{\text{scat}}^{\text{aer}}}{\tau_{\text{scat}}^{\text{aer}}} - \frac{\Delta\tau_{\text{ext}}^{\text{aer}}}{\tau_{\text{ext}}^{\text{aer}}} \approx \frac{\tau_{\text{scat}}^{\text{total}}}{\tau_{\text{scat}}^{\text{aer}}} \left\langle \frac{\Delta I(\Theta)}{I(\Theta)} \right\rangle - \frac{\Delta\tau_{\text{ext}}^{\text{total}}}{\tau_{\text{ext}}^{\text{aer}}}. \quad (10)$$

In addition, the errors in retrieved $\omega_0(\lambda)$ are anticorrelated with $\Delta\tau_{\text{ext}}^{\text{total}}$; that is, overestimation of $\tau(\lambda)$ results in underestimation of $\omega_0(\lambda)$. The errors in sky radiance $\Delta I(\Theta)/I(\Theta)$ are positively correlated with errors in retrieved $\omega_0(\lambda)$. Besides, the higher the aerosol optical thickness (both $\tau_{\text{scat}}^{\text{total}}$ and $\tau_{\text{scat}}^{\text{aer}}$), the smaller the error in retrieved $\omega_0(\lambda)$. These two tendencies are especially evident for water-soluble and biomass-burning aerosols. In the case of dust the effect of $\Delta\tau(\lambda)$ is very minor because $\tau(\lambda)$ is high for all wavelengths (see Table 3); however, the error in angular pointing strongly affects the estimates of $\omega_0(\lambda)$, similar to results for the retrieval of other dust optical characteristics. The underestimation of the scattering angle results in significant underestimation of $\tau_{\text{scat}}^{\text{aer}}$ because of the strong forward peak existing in sky radiances of the dust. This effect becomes smaller with increasing $\tau(\lambda)$ because the sharpness of the peak decreases owing to multiple-scattering effects.

The errors in a priori defined values of ground reflectance are anticorrelated with the errors appearing in the single-scattering albedo. This is because the inversion algorithm tends to compensate underestimation (overestimation) of ground albedo by an increase (decrease) of aerosol scattering (i.e., $\tau_{\text{scat}}^{\text{aer}}$ increases (decreases)).

Table 4 summarizes the results of tests for the retrieval sensitivity to the offsets. The errors in the estimates of size distribution are given for the values of $dV_i(r_i)/d \ln r$, which are not less than one tenth of the maximum. However, the error in estimating very small values $dV_i(r_i)/d \ln r$ (for example, the values on the tails of size distribution can be smaller than the maximum by a factor of 1000) can be much higher than 100% (which is the maximum error noted in Table 4). Table 4 does not include the errors caused by the maximum offsets ($\Delta\tau(\lambda) = \pm 0.02$) in $\tau(\lambda)$ for low optical depth situations

Table 4. Errors in the Size Distribution, Complex Refractive Index, and Single-Scattering Albedo

	Water-Soluble	Dust	Biomass Burning
$dV/d \ln r(r_i)$, %			
$0.1 \mu\text{m} < r < 7 \mu\text{m}$	15	35	25
$r < 0.1 \mu\text{m}$ and $r > 7 \mu\text{m}$	15–100	35–100	25–100
$n(\lambda)$			
$\tau_a(440) \leq 0.2$	0.05		
$\tau_a(440) > 0.2$	0.025		
$\tau_a(440) \geq 0.5$		0.04	0.04
$k(\lambda)$			
$\tau_a(440) \leq 0.2$	80–100%		
$\tau_a(440) > 0.2$	50%		
$\tau_a(440) \geq 0.5$		50%	30%
$\omega_0(\lambda)$			
$\tau_a(440) \leq 0.2$	0.05–0.07		
$\tau_a(440) > 0.2$	0.03		
$\tau_a(440) \geq 0.5$		0.03	0.03

Errors should be expected in the retrievals from the combination of spectral optical depth (440, 670, 870, and 1020 nm) and angular distribution of sky radiance in the solar almucantar (440, 670, 870, and 1020 nm; solar zenith angle of 60°) in the presence of the following instrumental offsets: in optical thickness, $\Delta\tau(\lambda) = \pm 0.01$; in sky radiances $I(\Theta; \lambda)$, $[\Delta_r(\Theta; \lambda)/I(\Theta; \lambda)] 100\% = \pm 5\%$; in azimuth angle pointing, $\Delta\phi = 0.5^\circ$; and in the a priori estimates of ground reflectance $A(\lambda)$, $[\Delta A(\lambda)/A(\lambda)] 100\% = \pm 50\%$.

and the errors caused by the maximum offsets in angular pointing ($\Delta\phi = 1^\circ$) for desert dust. These errors are excluded from this summary of the sensitivity tests because these errors are very high, and we expect to detect such situations from residual analysis (see section 3.4) and then exclude them from the AERONET-reported retrieval results. Also, we tested in detail only the situation with solar zenith angle equal to 60° , but we do not expect that dramatic differences will occur for the 50° – 70° solar zenith angle range.

3.3. Approximations in Forward Modeling and Selecting of Radiances

3.3.1. Approximations in forward modeling. The assumption of aerosol particles as homogeneous spheres is the strongest model restriction in the inversion procedure (Dubovik and King, submitted manuscript, 1999). Both assumptions of particle homogeneity and sphericity may not be valid. For example, in certain meteorological conditions the tropospheric aerosols present may be the result of different air mass interactions. Such aerosols may then be composed of a mixture of particles of different kinds. For example, dust or biomass-burning aerosols can be mixed with background water-soluble aerosol. Two different mechanisms of aerosol mixing can be expected: particles of different kinds interact or they do not interact. Correspondingly, in the case of noninteracting particles the particles of different kinds simply coexist, and no particles with new characteristics are formed. In this situation, particles of different sizes may have different values of the refractive indices. We will consider such a case as externally mixed particles. In the case of interacting particles, new kinds of particles with new optical characteristics can be formed. For example, small nonsoluble particles can be coated by water-soluble particles. As a result, after a certain period of aging, the mixed aerosol will consist of nonhomogeneous (internally mixed) particles, and special consideration is required [Ackerman and Toon, 1981]. For example, in the case of biomass-

burning aerosol the aerosol particles are expected to contain strongly absorbing impurities of soot rather than being homogeneous dielectric particles.

The shape of the particles becomes a critical issue for dust-like tropospheric aerosol, which consist of predominantly nonspherical particles [Koepke and Hess, 1988; Kaufman, 1993; Mishchenko et al., 1997]. This is why Mie scattering theory may not be appropriate for retrieval of desert dust optical properties.

Vertical variability of the atmosphere may also cause some errors in the retrieval results because inversions are implemented without accounting for detailed structure of the atmosphere. However, comparison of downward radiance simulated with and without accounting for vertical structure shows that the effect of these errors is modest in most simulations. Almost no effects of vertical structure can be observed for sky radiances in the solar almucantar. The radiances in the solar almucantar are the result of scattering and absorption by atmospheric layers viewed with similar geometry (zenith angle of observation is the same for all sky-measured radiances and equal to the solar zenith angle) and therefore not sensitive to the variations of vertical structure of atmospheric aerosol. This is why measurements in the solar almucantar are selected in the AERONET measurement protocol as the basic data for columnar aerosol retrieval.

3.3.2. Optimum selection of radiances. The retrieval uncertainties caused by modeling errors can likely be reduced if the inverted data set will include only measurements of radiances insensitive to the approximations employed in modeling these radiances. For example, the differences between spheres and nonspherical particles are minor at forward scattering angles [West et al., 1997], and the effects of multiple scattering and reflection from the ground are smaller in this region than for higher scattering angles [Kaufman et al., 1994]. Also, in the aureole angular range (scattering angles smaller than 40°), diffraction of light is a dominant scattering effect, which depends primarily on particle size and is independent of the refractive index [van de Hulst, 1957; Kaufman et al., 1994]. Therefore, if only sky radiances measured in the aureole are inverted, a good retrieval of particle sizes can be expected, even if assumptions on ground reflectance, particle composition, particle shape, etc., are not completely correct. From another side, limiting the inverted data set to only aureole data may increase the instability of the solution caused by random errors and measurement errors due to angular pointing. Correspondingly, further error analysis is focused on investigating the retrieval errors associated with limiting the data set to a specific angular range of inverted Sun-sky radiance. That is, we analyze the fruitfulness of inverting the sky radiance measured in a limited angular range instead of inverting the full almucantar. The following three angular ranges are considered: scattering angles $< 75^\circ$, 43° , and 30° . This analysis will also help to specify the accuracy of retrievals that would be obtained for the situations when Sun zenith angle is relatively small (35° and smaller), and sky radiances in correspondent solar almucantars will not contain measurements with large-scattering angles. In addition, for some cases we analyze the error changes associated with excluding the measurements of optical thickness from the inverted data set.

First, we evaluate the random error effects. According to the general conclusions of statistical estimation, reducing the number of measurements in the initial data set should result in a decrease of retrieval accuracy [cf. Edie et al., 1971]. However,

if the theoretically estimated decrease of retrieval accuracy is small, then the decrease of accuracy of the optical properties retrieved from the reduced initial data set is also expected to be small [see Dubovik *et al.*, 1995b]. Figure 8 illustrates how the retrieval errors caused by random errors change with the changes of angular range of the inverted data set. The errors are estimated according to (5) and (6). All figures show that reducing the data set angular range results in clear increases of the retrieval errors caused by random errors.

Second, we test how angular limiting of the inverted Sun-sky radiance data set changes the retrieval error caused by offsets. For these tests we implement all the calculations similar to the ones discussed in section 3.2.2. The only difference is that to reduce the tests to a reasonable number, we consider a singular situation for each aerosol model: water-soluble aerosol ($\tau(440) = 0.2$), dust ($\tau(440) = 0.5$), and biomass-burning aerosol ($\tau(440) = 1$). Selecting these three cases, we choose the optical thickness most typical for each kind of aerosol. The results of the tests are qualitatively similar to those displayed on Figure 8 and are not shown. All tests show that the angular restriction of inverted data does not improve the retrieval in the presence of offsets. Moreover, the opposite tendency is observed, whereby the retrieval error caused by offsets increases if we do not use spectral optical thickness data in the inversion or if we use sky radiances measured in the more narrow angular range. For example, a very poor retrieval of the real part of the refractive index is obtained for cases in which sky radiances measured in a limited angular range we used in the inversion. Correspondingly, we can conclude that in the presence of the instrumental offsets the real part of refractive index cannot be appropriately retrieved from sky radiances measured in a limited angular range. Alternatively, size distribution retrievals are satisfactory for all situations. These results are particularly important for the situation in which solar zenith angle, during the almucantar scan of AERONET Sun-sky radiometers, is significantly $< 60^\circ$, and hence the range of scattering angles necessary to yield a good estimate of the real part of the refractive index is not available.

3.3.3. External and internal mixtures of particles. The numerical tests described in section 3.3.2 show that in the cases in which the assumed approximations are sufficiently correct, any reduction of experimental input (angular limiting) will not make any improvements. However, this does result in significant decreases in solution stability due to the influence of random error. This is why the fruitfulness of the above data selection will depend on the prevalence of one of two competing tendencies: improving accuracy of the retrievals (due to decreasing model errors effects) and loss in stability of retrievals (due to increase of random noise destabilizing effect). It is expected that in some cases the errors caused by model approximations may have a negative impact on the retrieval, being occasionally much greater than the errors caused by random noise. Therefore, in section 3.3.3.1 we will test the errors that result because of model approximation of homogeneous and spherical particles.

3.3.3.1. External mixture: An external mixture of aerosol particles can be formed in very different ways. For example, more than two aerosols can be mixed together; each aerosol component may have a different particle size distribution; the particles of different components may differ in internal structure, shape, refractive indices, etc. In our studies we test only the simplest situation in which the fine and coarse modes represent the different aerosols composed of spherical and

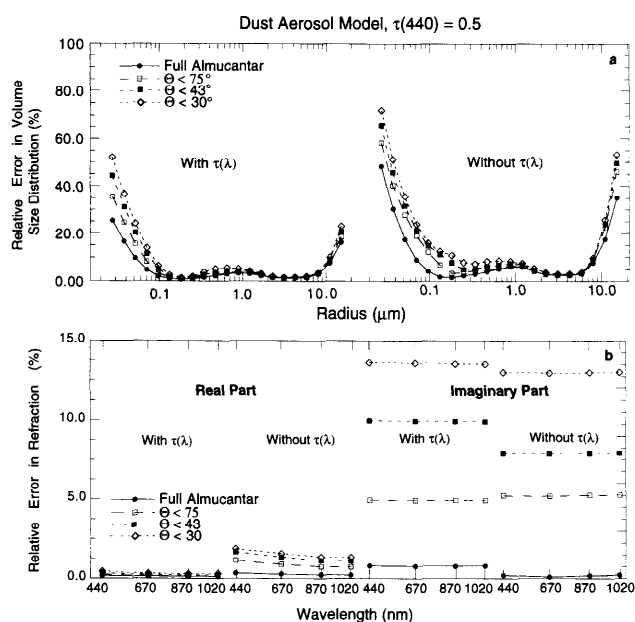


Figure 8. The standard deviation of the errors in estimates of volume size distribution and complex refractive index caused by random errors only. The different data sets are considered: sky radiance in full almucantar (scattering angle up to 120°) and limited by scattering angle 75° , 43° , or 30° with and without spectral optical thickness measurements. (a) The volume size distribution and (b) complex refractive index.

homogeneous particles, i.e., the fine and coarse modes of such a mixture of aerosol have similar spherical shape but different complex refractive indices. This simplest mixed aerosol may have rather different optical characteristics from the aerosol where all particles have the same refractive index. At the same time, if both fine and coarse modes are composed of two different kinds of particles with different refractive indices, the mixture may possibly have optical characteristics similar to the characteristics of homogeneous particles with effective complex refractive index. For testing our external mixture the size distributions of fine and coarse modes and the refractive index for the fine mode is assigned to be the same as in the water-soluble aerosol model (Table 2). The refractive index of the coarse mode is assigned as for dust (Table 2). In addition, we tested the case when particles of the fine and coarse modes have very different complex refractive indices: small particles have high real and imaginary parts of refractive index ($n(\lambda) = 1.65$; $k(\lambda) = 0.035$), and large particles have low real and imaginary parts of the refractive index ($n(\lambda) = 1.33$; $k(\lambda) = 0.0005$).

3.3.3.2. Internal mixture: An internal mixture of aerosol particles can also be influenced by various physical and chemical processes, which can result in particles with diverse internal structure and shape. The growth of such particles as well as their physical and optical parameters are widely discussed in the scientific literature [e.g., Ackerman and Toon, 1981; Draine and Flatau, 1994; Martins *et al.*, 1998]. In our tests we consider the simplest model of biomass-burning aerosol particles as layered spheres with black carbon core ($n(\lambda) = 1.65$; $k(\lambda) = 0.45$) surrounded by water-soluble substance ($n(\lambda) = 1.45$; $k(\lambda) = 0.0035$). We consider two kinds of layered spheres: The black carbon core has a fixed radius $r_{\text{core}} = 0.038 \mu\text{m}$ (the smaller particles are homogeneous black carbon particles), or

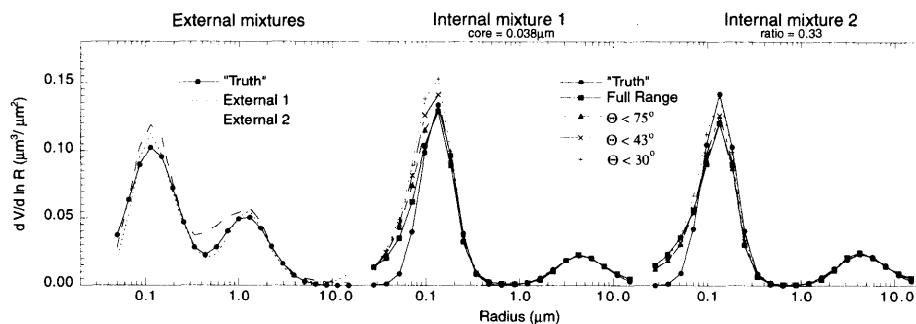


Figure 9. Volume size distributions of inhomogeneous aerosols (externally and internally mixed) retrieved using the model of scattering by homogeneous spheres.

the ratio between particle radius and radius of the core is fixed ($r_{\text{core}}/r_{\text{particle}} = 0.33$). The radius of the core and ratio are chosen so that the biomass-burning aerosol composed of internally mixed particles has a single-scattering albedo ($\omega_0(\lambda)$) quite similar to the single-scattering albedo of biomass-burning aerosol with the same size distribution but composed of homogeneous particles. The fixing of the same size distribution together with similar single-scattering albedo is necessary to provide practically realistic model of biomass-burning aerosol. For example, increasing (decreasing) the size of the absorbing core would result in unrealistically strong (weak) absorption of the aerosol. Figures 9 and 10 show the retrieval results for both cases of external and internal mixture, where the inversion code always assumes homogeneous spherical particles. The retrieved size distributions agree quite well with the assumed size distributions for all cases in Figure 9. The largest differences can be seen for the external mixture when fine and coarse have very different complex refractive indices. The retrieved real and imaginary parts of refractive indices correspond to certain effective values (Figure 10). These effective values can be close to the optical constants of the fine or coarse mode depending on the optical contribution of each mode to the total scattering. The retrieval results illustrated in Figure 10 show that the single-scattering albedo is retrieved rather well for both external and internal mixtures.

3.3.4. Nonspherical particles. For testing our retrieval algorithm in conditions of nonspherical scattering we use the model of desert dust given in the paper by *Mishchenko et al.* [1997], where the dust is considered as randomly oriented spheroids. We have simulated Sun and sky radiances using the T matrix code developed by *Mishchenko et al.* [1997] for prolate spheroids with semimajor/semiminor axis ratio of 2. To avoid serious numerical problems related to degenerated matrices appearing in modeled scattering by very large particles, we have restricted our consideration of particle size radii $< 2 \mu\text{m}$. A similar limit was used by *Mishchenko et al.* [1997]. Correspondingly, we chose a size distribution different from the one we used for spherical dust particles (dust 2 model in Table 2). This size distribution has a smaller mode radius of the coarse mode in comparison with the dust 1 model. In a series of sensitivity tests, the Sun and sky radiances simulated for this nonspherical dust model have been inverted by the code that assumes homogeneous spherical particles.

Figures 11 and 12 illustrate the results of these sensitivity tests for data sets with different angular range of sky radiance measurements. For sky radiance the relative random errors were assumed to have a 5% standard deviation. The random

errors in optical thickness were modeled as absolute errors with standard deviation equal to 0.01. The tests show that the correct shape of size distribution can be retrieved only in the cases when the limited angular range of sky radiance is used (scattering angles are $< 30^\circ$ – 40°). In the cases where the sky radiance corresponding to larger-scattering angles is used (especially for the case of the full almucantar) the retrieved size distribution shows a strong overestimation of the volume of fine particles. This result can easily be explained by the differ-

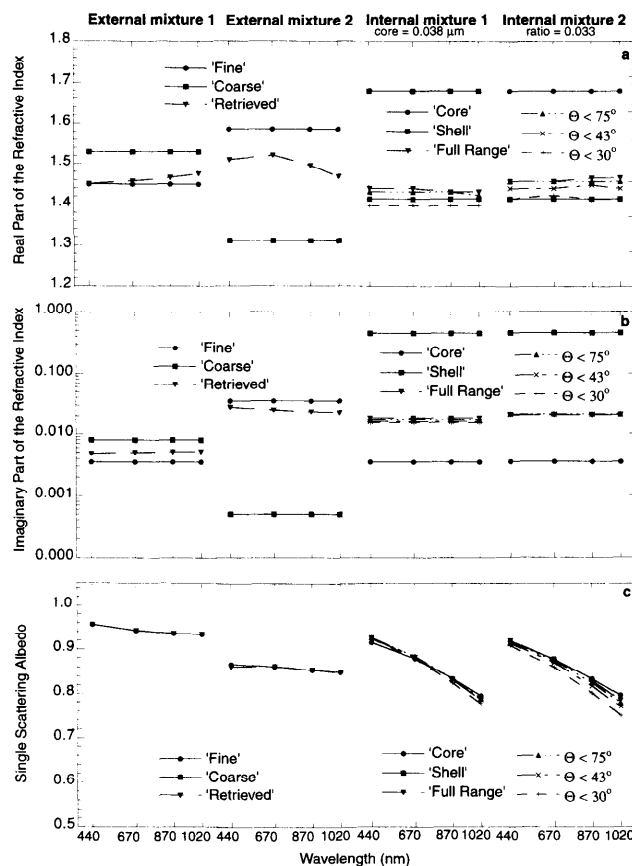


Figure 10. Complex refractive index and single-scattering albedo of inhomogeneous aerosol (externally and internally mixed aerosol) retrieved using the model of scattering by homogeneous spheres: (a) the real part of the refractive index, (b) the imaginary part of the refractive index, and (c) the aerosol single-scattering albedo.

ences in the phase functions of spheres and spheroids. The phase function of spheroids is significantly greater than the phase function of spheres in the middle range of angles between 70° and 150° [e.g., *Mishchenko et al.*, 1997]. Therefore the inversion code forces the appearance of false fine particles to compensate for the corresponding difference in sky radiances (Figure 12). For angles $<40^\circ$, there is almost no difference in the phase function of spheroids and spheres. This explains the better retrieval of the size distribution in the case when only aureole measurements of sky radiance are used (scattering angles $<30^\circ$ – 40°). However, even for these cases, we see some discrepancies, namely, the shape of the volume size distribution is retrieved correctly, but the volume of particles is overestimated.

This overestimation in volume size distribution retrieval arises from the fact that spheroids scatter more strongly than spheres of the same equivalent volume. For example, the extinction cross section in geometrical optics can be approximated as

$$Q_{\text{ext}}(r) = 2\bar{Q}_{\text{geom proj}}(r) = \frac{1}{2}S_{\text{surf}}(r), \quad (11)$$

where the extinction cross section $Q_{\text{ext}}(r)$ is expressed in terms $\bar{Q}_{\text{geom proj}}(r)$, the average geometrical projection of the spheroid (details are given by *Van de Hulst* [1957]). To relate the extinction cross section to the particle surface area $S_{\text{surf}}(r)$, we used the Cauchy theorem [*Vouk*, 1948], which establishes the relation between average geometrical projection and surface area of the spheroid as $\bar{Q}_{\text{geom proj}}(r) = \frac{1}{4}S_{\text{surf}}(r)$. Thus we conclude from the (11) that $Q_{\text{ext}}(r)$ for the randomly oriented spheroids is always higher than for volume-equivalent spheres because the sphere has the smallest surface area. Correspondingly, the algorithm based on scattering by spheres will always overestimate the absolute value of the volume concentration.

Figure 12 shows that the retrieved real and imaginary parts of the refractive index of spheres are rather different from the $n(\lambda)$ and $k(\lambda)$ used in most simulations. The retrieved real part of the refractive index has strong spectral dependence and is underestimated relative to modeled values in most of the cases. Only in the one case, when full range of sky radiances was inverted, were the values of $n(\lambda)$ at longer wavelengths (870 and 1020) close to the modeled values. The retrieved values of $k(\lambda)$ at all wavelengths are close to the modeled values within the 30% accuracy interval for the case when the

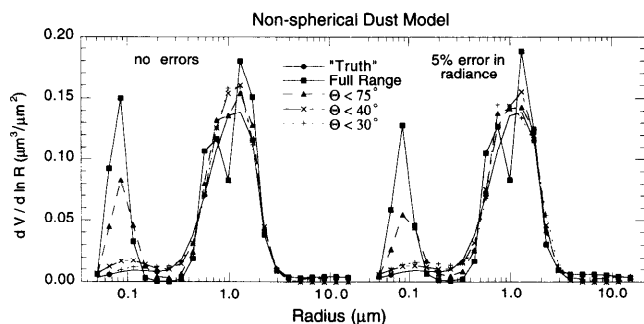


Figure 11. Volume size distributions of nonspherical aerosol particles retrieved using the model of scattering by homogeneous spheres. The different data sets used in the retrieval included spectral optical thickness measurements and sky radiance in full almucantar (scattering angle up to 120°), limited by scattering angles of 75° , 43° , or 30° .

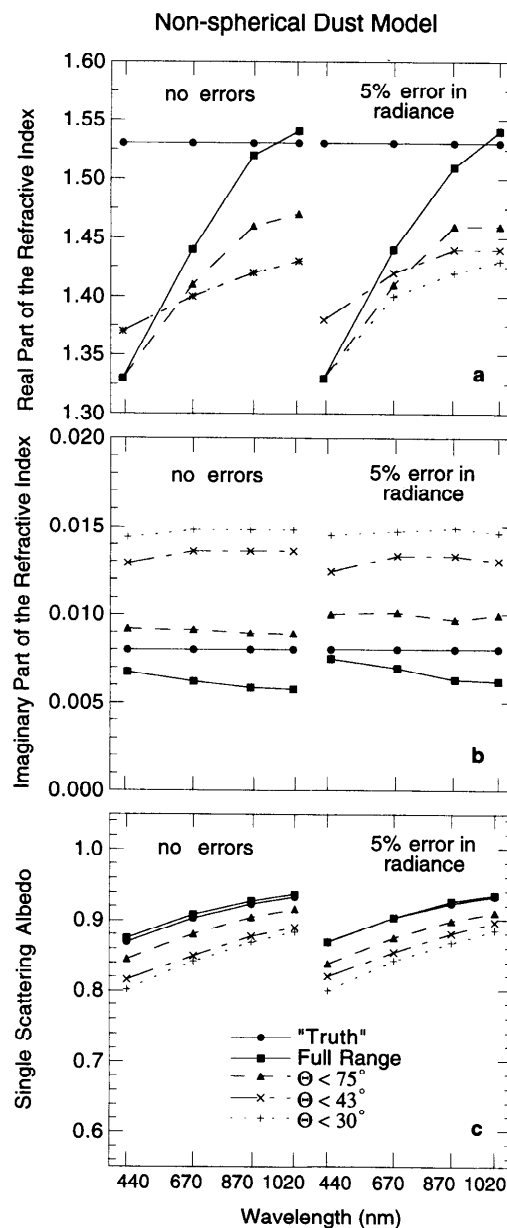


Figure 12. Complex refractive index and single-scattering albedo retrieval of nonspherical aerosol using the model of scattering by homogeneous spheres. The different data sets used in inversion include optical thickness measurements and sky radiance measurements in full almucantar (scattering angle up to 120°), limited by scattering angles 75° , 43° , or 30° : (a) the real part of the refractive index, (b) the imaginary part of the refractive index, and (c) the aerosol single-scattering albedo.

full range of sky radiances was inverted and when the angular range of inverted sky radiances covered all scattering angles up to 75° . The numerical tests show that the single-scattering albedo can be retrieved rather accurately if the basic data set (Sun radiances plus sky radiances in the whole almucantar) is inverted (Figure 12). It is known from direct simulations that nonspherical scattering does not result in large changes of single-scattering albedo [*Koepke and Hess*, 1988; *Mishchenko et al.*, 1997]; that is, nonspherical scattering does not significantly change the proportion between total scattering and total extinction $\omega_0(\lambda) = \tau_{\text{scat}}/\tau_{\text{ext}}$. However, in our opinion, this con-

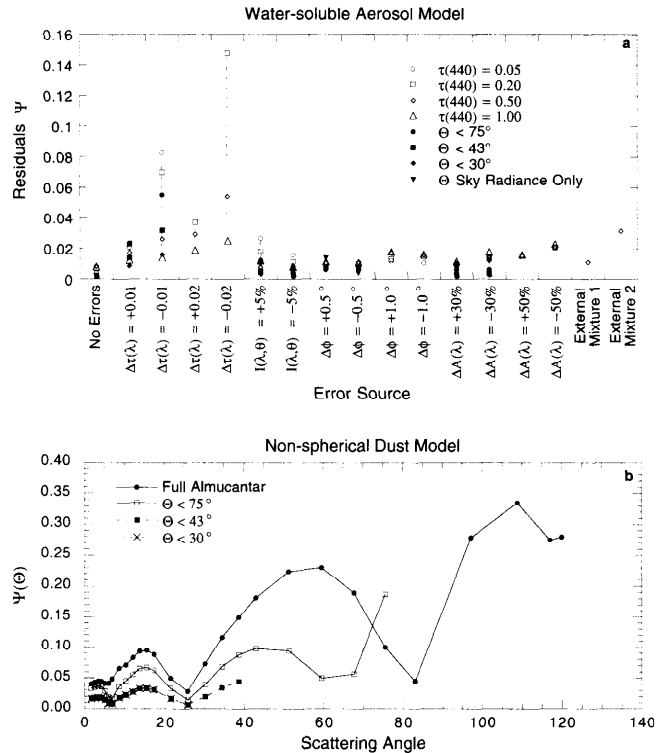


Figure 13. The residuals (calculated by (6)) observed in sensitivity test: (a) the residuals (calculated by (6)) for model of water-soluble aerosol and (b) the angular dependence of the residual of the sky radiances ($\Psi(\theta) = [I_{\text{meas}}(\theta) - I_{\text{fitted}}(\theta)]/I_{\text{meas}}(\theta)$) observed in the retrieval of nonspherical dust using the model of homogeneous spherical aerosol particles.

clusion can hardly be considered as a guarantee of a good retrieval of single-scattering albedo from Sun-sky radiances. Indeed, forward simulations usually are comparing the single-scattering albedo of nonspherical and spherical particles having the same size distribution and refractive index. At the same time, the inversion process allows the fitting of Sun-sky radiances by the spheres with a different size distribution and different refractive index, possibly leading to different single-scattering albedo results. Such situations can be seen for all retrievals where the whole almucantar is not used. The main problem in single-scattering albedo retrieval is to correctly derive the total scattering τ_{scat} (the extinction optical thickness τ_{ext} is measured directly):

$$\tau_{\text{scat}}(\lambda) = \frac{1}{2} \int_0^\pi \tau_{\text{scat}}(\lambda) P_\lambda(\theta) \sin(\theta) d\theta. \quad (12)$$

From this equation we see that if the sky radiances are fitted accurately in the whole range of available scattering angles (i.e., the values $\tau_{\text{scat}}(\lambda)P_\lambda(\theta)$ are approximated as accurately as possible by Mie scattering), the estimates of τ_{scat} should also be accurate. At the same time, it is important to use the whole range of available scattering angles (from 2° to 120°) because in this angular range the phase function of nonspherical particles is smaller than the Mie phase function in the forward hemisphere and larger in the backward hemisphere. Correspondingly, if only a very limited angular range ($<30^\circ$, 40° , or 75°) is used, τ_{scat} can be underestimated. It should be noted that lack

of sky radiances corresponding to angles $>120^\circ$ does not affect the retrieval of single-scattering albedo because the contribution of these angles to the total scattering τ_{scat} is very minor owing to $\sin(\theta)$ response in (12). Additional discussion concerning the importance of the angular range for single-scattering albedo retrieval is given by Dubovik *et al.* [1998a].

3.4. Residuals

The inversion is designed as a search for the best fit solution, i.e., the minimization of $\Psi_{\text{min}}(\mathbf{a})$ (equation (4)). The value of the smallest residual $\Psi_{\text{min}}(\mathbf{a})$ is sensitive to the presence of errors in the experimental data. Therefore this value is usually employed as an indicator of the retrieval quality, similar to what is done in (6). However, this equation is formulated to evaluate only random errors under the assumption of no systematic errors. Nevertheless, it is our anticipation that (6) can indicate the retrieval quality in the presence of systematic errors or failure of the radiative model because not all systematic errors in Sun-sky radiances can be fitted by the forward model without any residual (i.e., $\Psi(\mathbf{a}) = 0$). This is true especially for the case when the total number of measurements in Sun-sky radiance data set is larger than the total number of retrieved unknown parameters because not all changes in Sun-sky radiances are compatible.

To evaluate the sensitivity of the residual $\Psi(\mathbf{a})$ to systematic errors, we controlled the value $\hat{\epsilon}_1$ estimated by (6) in all numerical tests. Figure 13a shows the residuals that were obtained in all tests for water-soluble aerosol (the results for dust and biomass-burning aerosols are not shown). A clear increase of the residual can be observed for the cases with high relative error in the measurements of optical depth, i.e., for water-soluble aerosol (in Figures 3 and 4, $\tau(440) = 0.05$ and 0.2) and for biomass-burning aerosol. For the case of dust the residual increases for the case of systematic error in angular pointing and, especially, for the case of nonspherical particles. Thus the residual increases significantly for all cases with a strong influence of systematic errors; that is, there is a clear correlation between the accuracy of the retrieval and the value of $\Psi(\mathbf{a})$. Correspondingly, the error estimated by (5) and (6) should be sensitive to systematic errors affecting the retrieval accuracy, and they can indicate an increase in the retrieval errors over the values given in Table 4.

Also, for the case of nonspherical scattering (Figure 13b) the increase of the residual arises for the case when sky radiances in the full almucantar are used. This residual increase almost disappears with a decrease of angular range of inverted sky radiances. It should be noted that for the case of nonspherical scattering the fitting accuracy of the sky radiances $[I_{\text{meas}}(\theta) - I_{\text{fitted}}(\theta)]/I_{\text{meas}}(\theta)$ shows a very well pronounced decrease for large-scattering angles (Figure 13b). Therefore this increase can be used as an indicator of the presence of significant nonspherical scattering.

4. Summary and Conclusion

In this paper we described the results of our sensitivity studies to assess the accuracy of our new method for deriving aerosol optical properties from inversion of Sun-sky radiance measurements. The method is based on the inversion algorithm developed by Dubovik and King (submitted manuscript, 1999) that allows global fitting of spectral and multiangle Sun-sky radiances with a simultaneous search for the aerosol size distribution and complex refractive index. We tested the re-

retrieval accuracy of these parameters as well as aerosol single-scattering albedo in the presence of random and systematic errors. The analysis was focused on inverting the data combination typically measured by AERONET radiometers: spectral optical thickness in four wavelengths together with the angular distribution of sky radiance in the solar almucantar at the same wavelengths. Additionally, we clarified the significance of using sky radiances corresponding to large-scattering angles (75° and larger). This aspect of the studies was important to both identify the best combination of Sun-sky radiances for the retrieval and to recognize accuracy differences in the inversions of the solar almucantars corresponding to different solar zenith angles (i.e., different scattering angular coverage).

To evaluate the errors caused by random noise, the linear error estimates given by (5) and (6) were tested. The effects of systematic errors, which cannot be considered as random errors, were analyzed separately. Sun or sky channel miscalibration, inaccurate pointing of emergent azimuth angle during sky radiance measurements, and inaccuracy in accounting for ground reflectance were considered as possible systematic offsets in the inverted radiance data. The effects of these errors on the characterization of three typical and optically distinct bimodal aerosols (weakly absorbing water-soluble aerosol, absorbing biomass-burning aerosol, and dust) were considered. The major noticed difficulties related to the characterization of aerosol under very low optical thickness conditions. A particularly distinct increasing of retrieval errors with decreasing τ_{ext} has been observed for the retrieval of the refractive index and aerosol single-scattering albedo. For the retrieval of the size distribution, a similar tendency exists but less pronounced. The accurate azimuth angle pointing is critical for the characterization of dust. Limitation of the angular coverage of measured sky radiance (from scattering angles out to 120° down to maximum scattering angles 75°, 40°, and 30°) results in a dramatic decrease in retrieval accuracy for the real part of the refractive index and some decrease of the retrieval accuracy for other parameters (the smallest effect is on the size distribution). Quantitative estimates of the accuracy of the retrieval using both spectral optical thickness and sky radiance measured in the full solar almucantar (solar zenith angle of 60°) are summarized in Table 4.

In the retrieval the aerosol particles are assumed to be polydisperse homogeneous spheres that have the same complex refractive index. Therefore we examined how much these assumptions mislead our inversion solutions in the case of nonspherical dust aerosols and in the case of externally or internally mixed spherical particles with different refractive indices. For both cases of internally and externally mixed particles, no significant errors were observed in the retrieval of single-scattering albedo. The retrieved size distributions also agree quite well with the assumed size distributions for all cases of mixed particles. The largest differences were found for an external mixture of particles in which fine and coarse mode particles have very different complex refractive indices. The retrieved real and imaginary parts of the refractive indices correspond to effective values in between those assumed in the inhomogeneous particles. For nonspherical particle scattering the tests show that the shape of size distribution can be retrieved only in cases where the angular range of sky radiance is limited to scattering angles are <30°–40°. However, the single-scattering albedo can be retrieved rather accurately only if the complete basic data set (Sun radiances plus sky radiances in the whole almucantar) is inverted. The real part of the refrac-

tive index of nonspherical particles cannot be retrieved with good accuracy using Mie scattering (the real part of the refractive index is underestimated in most cases). Nevertheless, the values of $n(\lambda)$ retrieved from the complete basic data set are close to the real values at longer wavelengths (870 and 1020 nm). The values of the imaginary part of the complex refractive index can be retrieved with an accuracy of 30% in cases where the angular range of sky radiance is fit up to scattering angles of 75° or larger.

In addition, it is shown that the minimum value of the residual given by (5) and (6) (the best fit of measured radiances to a theoretical model) is sensitive to both the presence of experimental error and the failure of the radiative model. Therefore this residual value can be adopted as an indicator of the quality of the retrieval.

Acknowledgments. The authors are grateful to Alexander Kostinski, Robert S. Fraser, and Didier Tanre for valuable discussions and help in improving the paper. We thank Robert Curran of NASA Headquarters for his support. We thank two anonymous reviewers for their detailed and constructive comments.

References

- Ackerman, T. P., and O. B. Toon, Absorption of visible radiation in atmosphere containing mixtures of absorbing and nonabsorbing particles, *Appl. Opt.*, **20**, 3661–3668, 1981.
- Bohren, C. F., and D. R. Huffman, *Absorption and Scattering of Light by Small Particles*, 550 pp., John Wiley, New York, 1983.
- Dave, J. V., Importance of higher order scattering in a molecular atmosphere, *J. Opt. Soc. Am.*, **54**, 307–315, 1964.
- Deering, D. W., Field measurements of bidirectional reflectance, in *Theory and Applications of Optical Remote Sensing*, edited by G. Asrar, pp. 14–65, John Wiley, New York, 1989.
- Devaux, C., A. Vermeulen, J. L. Deuze, P. Dubuisson, M. Herman, and R. Santer, Retrieval of aerosol single-scattering albedo from ground-based measurements: Application to observational data, *J. Geophys. Res.*, **103**, 8753–8761, 1998.
- Draine, B. T., and P. J. Flatau, Discrete dipole approximation for scattering calculations, *J. Opt. Soc. Am. A Opt. Image Sci.*, **11**, 1491–1499, 1994.
- Dubovik, O. V., T. V. Lapyonok, and S. L. Oshchepkov, Improved technique for data inversion: Optical sizing of multicomponent aerosols, *Appl. Opt.*, **34**, 8422–8436, 1995a.
- Dubovik, O. V., T. V. Lapyonok, and S. L. Oshchepkov, Improved technique for statistically optimum inversion of optical data in presence of measurements and model noise, in *Passive Infrared Remote Sensing of Clouds and Atmosphere 2*, edited by David K. Lynch, *Proc. SPIE Int. Soc. Opt. Eng.*, **2309**, 184–195, 1995b.
- Dubovik, O., B. N. Holben, Y. J. Kaufman, M. Yamasoe, A. Smirnov, D. Tanré, and I. Slutsker, Single-scattering albedo of smoke retrieved from the sky radiance and solar transmittance measured from ground, *J. Geophys. Res.*, **103**, 31,903–31,924, 1998a.
- Dubovik, O., T. Yokota, and Y. Sasano, Improved technique for data inversion and its application to the retrieval algorithm for ADEOS/ILAS, *Adv. Space Res.*, **21**(103), 397–403, 1998b.
- Eck, T. F., B. N. Holben, J. S. Reid, O. Dubovik, S. Kinne, A. Smirnov, N. T. O'Neill, and I. Slutsker, The wavelength dependence of the optical depth of biomass burning, urban and desert dust aerosols, *J. Geophys. Res.*, **104**, 31,333–31,350, 1999.
- Edie, W. T., D. Dryard, F. F. James, M. Roos, and B. Sadoulet, *Statistical Methods in Experimental Physics*, 155 pp., North-Holland, New York, 1971.
- Holben, B. N., D. Tanré, Y. Kaufman, I. Slutsker, and D. Ward, Single-scattering albedo approximated from ground based measurements of aerosol optical thickness in the Amazon Basin, in *SCAR-B Proceedings*, edited by V. Kirchoff, pp. 73–77, Transtec Edit., São Paulo, Brazil, 1996.
- Holben, B. N., et al., AERONET—A federated instrument network and data archive for aerosol characterization, *Remote Sens. Environ.*, **66**, 1–16, 1998.

- Kaufman, Y. J., Aerosol optical thickness and atmospheric path radiance, *J. Geophys. Res.*, **98**, 2677–2992, 1993.
- Kaufman, Y. J., A. Gitelson, A. Karnieli, E. Ganor, R. S. Fraser, T. Nakajima, S. Mattoo, and B. N. Holben, Size distribution and scattering phase function of aerosol particles retrieved from sky brightness measurements, *J. Geophys. Res.*, **99**, 10,341–10,356, 1994.
- Kaufman, Y. J., D. Tanré, H. R. Gordon, T. Nakajima, J. Lenoble, R. Frouin, H. Grassl, B. M. Herman, M. D. King, and P. M. Teillet, Passive remote sensing of tropospheric aerosol and atmospheric correction for the aerosol effect, *J. Geophys. Res.*, **102**, 16,815–16,830, 1997.
- King, M. D., D. M. Byrne, B. M. Herman, and J. A. Reagan, Aerosol size distributions obtained by inversion of spectral optical depth measurements, *J. Atmos. Sci.*, **21**, 2153–2167, 1978.
- King, M. D., Y. J. Kaufman, D. Tanré, and T. Nakajima, Remote sensing of tropospheric aerosols from space: Past, present, and future, *Bull. Am. Meteorol. Soc.*, **80**, 2229–2259, 1999.
- Koepke, P., and M. Hess, Scattering functions of tropospheric aerosols: The effects of nonspherical particles, *Appl. Opt.*, **27**, 2422–2430, 1988.
- Martins, J. V., P. Artaxo, C. Liousse, J. S. Reid, P. V. Hobbs, and Y. J. Kaufman, Effects of black carbon content, particle size, and mixing on light absorption by aerosol from biomass burning in Brazil, *J. Geophys. Res.*, **103**, 32,041–32,050, 1998.
- Mishchenko, M. I., L. D. Travis, R. A. Kahn, and R. A. West, Modeling phase functions for dustlike tropospheric aerosols using a shape mixture of randomly oriented polydisperse spheroids, *J. Geophys. Res.*, **102**, 16,831–16,847, 1997.
- Nakajima, T., and M. Tanaka, Algorithms for radiative intensity calculations in moderately thick atmospheres using a truncation approximation, *J. Quant. Spectrosc. Radiat. Transfer*, **40**, 51–69, 1988.
- Nakajima, T., M. Tanaka, and T. Yamauchi, Retrieval of the optical properties of aerosols from aureole and extinction data, *Appl. Opt.*, **22**, 2951–2959, 1983.
- Nakajima, T., G. Tonna, R. Rao, P. Boi, Y. Kaufman, and B. Holben, Use of sky brightness measurements from ground for remote sensing of particulate polydispersions, *Appl. Opt.*, **35**, 2672–2686, 1996.
- O'Neill, N. T., and A. Royer, Extraction of bimodal aerosol-size distribution radii from spectral and angular slope (Ångström) coefficients, *Appl. Opt.*, **32**, 1642–1645, 1993.
- Phillips, B. L., A technique for numerical solution of certain integral equation of first kind, *J. Assoc. Comp. Mach.*, **9**, 84–97, 1962.
- Ranson, K. J., J. R. Irons, and D. L. Williams, Multispectral bidirectional reflectance of northern forest canopies with Advanced Solid-State Array Spectroradiometer (ASAS), *Remote Sens. Environ.*, **47**, 276–289, 1994.
- Reagan, J. A., L. W. Thomason, B. M. Herman, and J. M. Palmer, Assessment of atmospheric limitations on the determination of the solar spectral constant from ground-based spectra radiometer measurements, *IEEE Trans. Geosci. Remote Sens.*, **GE-24**, 258–265, 1986.
- Remer, L. A., Y. J. Kaufman, B. N. Holben, A. M. Thompson, and D. P. McNamara, Biomass burning aerosol size distribution and modeled optical properties, *J. Geophys. Res.*, **103**, 31,879–31,891, 1998.
- Rodgers, C. D., Retrieval of atmospheric temperature and composition from remote measurements of thermal radiation, *Rev. Geophys.*, **14**, 609–624, 1976.
- Russell, P. B., et al., Pinatubo and pre-Pinatubo optical depth spectra: Mauna Loa measurements, comparisons, inferred particle size distributions, radiative effects, and relationship to lidar data, *J. Geophys. Res.*, **98**, 22,969–22,985, 1993.
- Shaw, G. E., Error analysis of multi-wavelength sun photometry, *Pure Appl. Geophys.*, **114**, 1–14, 1976.
- Smirnov, A., B. N. Holben, T. F. Eck, O. Dubovik, and I. Slutsker, Cloud screening and quality control algorithms for the AERONET data base, *Remote Sens. Environ.*, in press, 2000a.
- Smirnov, A., B. N. Holben, O. Dubovik, N. T. O'Neill, L. A. Remer, T. F. Eck, I. Slutsker, and D. Savoie, Measurement of atmospheric optical parameters on U.S. Atlantic coast sites, ships, and Bermuda during TARFOX, *J. Geophys. Res.*, in press, 2000b.
- Soulen, P. F., M. D. King, S. C. Tsay, G. T. Arnold, and J. Y. Li, Airborne spectral measurements of surface anisotropy during the SCAR-A, Kuwait oil fire, and TARFOX experiment, *J. Geophys. Res.*, in press, 2000.
- Stamnes, K., S. C. Tsay, W. Wiscombe, and K. Jayaweera, Numerically stable algorithm for discrete ordinate-method radiative transfer in multiple scattering and emitting layered media, *Appl. Opt.*, **27**, 2502–2509, 1988.
- Tanré, D., L. R. Remer, Y. J. Kaufman, S. Mattoo, P. V. Hobbs, J. M. Livingston, P. B. Russell, and A. Smirnov, Retrieval of aerosol optical thickness and size distribution over ocean from the MODIS airborne simulator during TARFOX, *J. Geophys. Res.*, **104**, 2261–2278, 1999.
- Tikhonov, A. N., On the solution of incorrectly stated problems and a method of regularization, *Dokl. Akad. Nauk.*, **151**, 501–504, 1963.
- Tsay, S. C., M. D. King, G. T. Arnold, and J. Y. Li, Airborne spectral measurements of surface anisotropy during SCAR-B, *J. Geophys. Res.*, **103**, 31,943–31,954, 1998.
- Twomey, S., On the numerical solution of Fredholm integral equations of the first kind by the inversion of the linear system produced by quadrature, *J. Assoc. Comp. Mach.*, **10**, 97–101, 1963.
- Twomey, S., *Introduction to the Mathematics of Inversion in Remote Sensing and Indirect Measurements*, 243 pp., Elsevier Sci., New York, 1977.
- van de Hulst, H., *Light Scattering by Small Particles*, 370 pp., John Wiley, New York, 1957.
- Vouk, V., Projected area of convex bodies, *Nature*, **162**, 330–331, 1948.
- Wendish, M., and W. von Hoyningen-Huene, Possibility of refractive index determination of atmospheric aerosol particles by ground-based solar extinction and scattering measurements, *Atmos. Environ.*, **28**, 785–792, 1994.
- West, R. A., L. R. Doose, A. M. Eibl, M. G. Tomasko, and M. I. Mishchenko, Laboratory measurements of mineral dust scattering phase function and linear polarization, *J. Geophys. Res.*, **102**, 16,871–16,881, 1997.
- Yamasoe, M. A., Y. J. Kaufman, O. Dubovik, L. A. Remer, B. N. Holben, and P. Artaxo, Retrieval of the real part of the refractive index of smoke particles from Sun/sky measurements during SCAR-B, *J. Geophys. Res.*, **103**, 31,893–31,902, 1998.

O. Dubovik, T. F. Eck, B. N. Holben, I. Slutsker, and A. Smirnov, Laboratory for Terrestrial Physics, NASA Goddard Space Flight Center, Code 923, Greenbelt, MD 20771. (dubovik@spamer.gsfc.nasa.gov)
 Y. J. Kaufman, Laboratory for Atmospheres, NASA Goddard Space Flight Center, Code 913, Greenbelt, MD 20771.
 M. D. King, Earth Science Directorate, NASA Goddard Space Flight Center, Code 900, Greenbelt, MD 20771.

(Received May 11, 1999; revised December 20, 1999; accepted December 21, 1999.)